UNIVERSITY OF CALIFORNIA SAN DIEGO

Advantages and Limitations of Bio-polymer Treatments for Remediation of Wildfire Burned Slopes and Prevention of Post-wildfire Mudflows

A Thesis submitted in partial satisfaction of the requirements
for the degree Master of Science

in

Structural Engineering

by

Jonathon Chavez De Rosas

Committee in charge:

Professor Ingrid Tomac, Chair
Professor Ahmed Elgamal
Professor John McCartney

2022

The Thesis of Jonathon Chavez De Rosas is approved, and it is acceptable in quality and form for publication on microfilm and electronically.

University of California San Diego

2022

TABLE OF CONTENTS

LIST OF FIGURES

LIST OF TABLES

ACKNOWLEDGEMENTS

I would like to acknowledge Professor Ingrid Tomac for her support throughout the research and my graduate program. Her guidance and advice were crucial to my success.

Chapter 1, in part, has been submitted for publication of the material as it may appear in Journal of Geotechnical and Geoenvironmental Engineering, Chavez De Rosas, Jonathon; Tomac, Ingrid, 2022. The thesis author was the primary researcher and author of this paper.

Chapter 2, in part, is currently being prepared for submission for publication of the material. Chavez De Rosas, Jonathon; Tomac, Ingrid. The thesis author was the primary researcher and author of this material.

ABSTRACT OF THE THESIS

Advantages and Limitations of Bio-polymer Treatments for Remediation of Wildfire Burned Slopes and Prevention of Post-wildfire Mudflows

by

Jonathon Chavez De Rosas

Master of Science in Structural Engineering

University of California San Diego, 2022

Professor Ingrid Tomac, Chair

Wildfire frequency has recently increased due to climate change and anthropogenic factors, carrying along post-wildfire mud and debris flow risk. Burned scars with hydrophobic topsoil layers and without vegetation erode rapidly in rain, carrying large boulders and debris downhill.

Recently, improved remediation techniques using biopolymers have been proposed for temporary protection of burned scars against erosion, until recovery and vegetation regrowth. This thesis investigates experimentally the advantages and limitations of xanthan gum (XG) biopolymer slope improvement. Among several different XG application techniques investigated, the best results against erosion were achieved with a pluviated XG and hydrophilic sand mix, cured by water spraying. For example, a 15-min 50 mm/hr rain led to a catastrophic erosion of the uncured XG mix, while the cured 1-3% XG mix protected slopes. Results showed that sand type is a governing parameter and fine sands require high XG content for soil improvement, unlike coarse sands. Results also identified surface morphology evolution, with ridges, that can fail during prolonged rain. Concurrently, six slopes with all three sand types at two different angles were exposed to natural environments and nine rain events. Initial treatments of uncured 0.5% XG mixed with sand did not reduce erosion, forming deep channels in the slopes by the fifth rain event. Re-covering the slopes with a 3% XG-sand mix and curing performed better at higher rain intensities but experienced heightened erosion in channels. Recommendations and guidelines are given for optimal XG use across different sand types, rain intensities, and slope angles.

INTRODUCTION

This work presents a comprehensive experimental investigation of the advantages and limitations of biopolymer, specifically xanthan gum, to reduce susceptibility or prevent post-wildfire rain-induced hillslope erosion. Water-repellency, or hydrophobicity, exists in minimal quantities in natural mineral forest soils but does not affect the soil cover permeability (DeBano 1981; Doerr et al. 2000; Huffman et al. 2001). However, the hydrophobicity significantly intensifies when a wildfire vaporizes and condenses fuel burn compounds into the surrounding soil. As a result, a newly post-wildfire formed surficial hydrophobic soil layer substantially reduces the infiltration of rainwater and promotes surface erosion (DeBano and Krammes 1966; DeBano 1967; Meeuwig 1971; Savage 1974; Helvey 1980; DeBano 1981; Scott and Van Wyk 1990; Crockford et al. 1991; Doerr et al. 1996; Huffman et al. 2001). Furthermore, wildfire frequency has been exponentially rising. For example, in 2021, California (CA), US had 8,786 fires burning a total of over 2.5 million acres, posing a threat of mudflows over burn scars following a fire (Department of Forestry and Fire Protection 2022). Mudflows in California, US were triggered in 2021 with rain intensities as low as 8.89 mm/hr (Department of Forestry and Fire Protection 2022).

Xanthan gum (XG) reduces the permeability of sandy soils by filling pores (Gioia and Ciriello 2006). For example, Ayeldeen et al. (2016) determined the coefficient of permeability for sands decreased to 4% of its original untreated value at 2% XG concentration by weight after five weeks of curing. The longer the sand cures, the more permeability and hydraulic conductivity decrease, as the XG-particle links change from a gel to thinner glass-like strands (Ayeldeen et al. 2016; Cabalar et al. 2017; Moghal and Vydehi 2021). Apart from decreasing permeability, biopolymer allows the soil to retain more water due to strong hydrogen bonding (Khachatoorian

et al. 2003). In addition, the reduced permeability leads to soil plugging effects, aiding with soil remediation (Khachatoorian et al. 2003). When looking for vegetation growth improvement in drylands, just 0.5% XG implemented into the soil is enough to stimulate vegetation growth (Tran et al. 2019). The compressive strength of saturated, poorly graded Sydney sand and well-graded low-plasticity residual Piedmont soils mixed with XG increases (Lee et al. 2019; Soldo et al. 2020). For example, the 16.5% void ratio saturated soil compressive strength increases from 181 kPa to 3348 kPa, 5989 kPa, and 6185 kPa for 1%, 2%, and 4% concentration after five days of curing, respectively, with a slight decrease in strength for the 1% and 2% concentrations after 30 days (Soldo et al. 2020). Dry blending mixes and coats the surface of the particles with the biopolymer, including clays or silicate nanocomposites (Alexandre and Dubois 2000; Akin and Likos 2016).

XG has been used in several studies to control and mitigate wind and water erosion on slopes. For example, Kavazanjian Jr. et al. (2009) conducted wind experiments using an aluminum conduit and a fan to expose biopolymer-treated sands to approximately 26 km/hr airflow velocity. By applying an XG emulsion with a spray bottle, the soil loss percentage of experiments using 0.5% XG concentration was lowered to 0.04% from 32% observed with untreated sand. Mahayama et al. (2021) found fly ash treated with 1% XG remained undamaged, making it a suitable protective method against wind erosion, like previous work done by Chen et al. (2015), which determined mine tailings treated with biopolymers increased the penetration force. Movasat and Tomac (2020) distributed a 4% by weight ratio of XG to base hydrophobic sand, raining over it for 100 min and collecting overflown water and eroded sand every 10 minutes. They found that the water runoff generally increased in the XG treated slopes while observing a vastly decreased soil erosion in the treated sand. Akin et al. (2021) drew the same conclusions for a slightly different setup, raining on the treated hydrophobic soil slopes sprinkled with 2.8 g of XG uniformly on a

compacted soil surface for 30 min with a rain intensity of 102 mm/hr, drying, and repeating the cycle two more times. Mahayama et al. (2021) qualitatively found that fly ash and overburden mine soil were stabilized against water erosion with as little as 1% concentration of XG, with similar results found by Joga and B. J. S. (2020) for two soil types in Karnataka, India. Biopolymer increases the surface erosion resistance by reducing the erodibility coefficient from 9,132 mm/hr to 1,100 mm/hr in the specimen containing the highest sucrose concentration, stimulating the biopolymer dextran growth (Ham et al. 2018). The decrease in the erodibility coefficient is due to the shear strength increase from cohesion. Thus, a similar conclusion can be drawn for XG as Soldo et al. (2020) found the cohesion increased by a factor of 3.2 after five days of curing.

Erosion of burned scars is triggered by rainfall. An overview of recent rain types and intensities that led to post-wildfire debris flow reveals a wide range. For example, in 2018 in Montecito, CA, the highest average hourly rainfall intensity was slightly higher than 10 mm/hr, with an instantaneous rainfall intensity jump to 50 mm/hr a few minutes before the debris flow occurred (Tiwari et al. 2020). The cumulative rainfall over the three-day storm was around 37.5 mm. Oakley et al. (2017) synthesized post-fire debris flows from 19 precipitation events ranging from 1980 to 2014 due to atmospheric rivers (ARs) and closed lows. ARs, defined as narrow regions of enhanced water vapor transport in the lower troposphere, can increase precipitation in mountain ranges at landfall (Ralph et al. 2016). Closed lows are low-pressure areas with a distinct center of cyclonic circulation that one or more height contours can completely encircle (Oakley and Redmond 2014; NOAA 2011). Within the 19 precipitation events studied, ARs were the atmospheric event for 11 out of 19, with the lowest rainfall range being 5-11 mm/hr, and 21 mm/hr when observed over 15 minutes taking place in La Cañada Flintridge, CA, on December 12, 2009, within the Station burn scar. The highest average rainfall rate was 5-33 mm/hr in San Bernardino,

CA, on December 25, 2003, within the Grand Prix and Old fire burn scars. Debris flows occurred within the Springs burn scar in the Santa Monica Mountains, CA, triggered by a 15-minute rain intensity of 15 mm/hr on December 12, 2014 (Oakley et al. 2017).

CHAPTER 1: EXPERIMENTAL INVESTIGATION OF ADVANTAGES AND LIMITATIONS OF XANTHAN GUM FOR POST-WILDFIRE SURFACE EROSION CONTROL

1.1 INTRODUCTION

Although previous studies showed the effects of biopolymers on improving sand shear strength and decreasing permeability, a limited number of studies use biopolymers as a post-wildfire slope mitigation technique, leaving much unknown. Furthermore, little research focused on improving erosion by covering hydrophobic slopes with pure XG, without exploring alternative application approaches. Therefore, this chapter focuses on gaps in the literature regarding the effects of sand type and particle size, rain intensity, slope angle, and XG concentration, including the coupling of relevant parameters, for mitigation of post-wildfire slopes, as well as advantages and limitations of the method.

1.2 METHODOLOGY

This research's experiments and analysis systematically investigate the advantages and limitations of XG effectiveness for remediation of wildfire burned sandy slopes. The experimental program includes investigating coupled effects of anticipated rain intensity, slope inclination, XG application technique, and XG percentages effects on susceptibility of erosion and erosion protection of fine, medium, and coarse sand.

1.2.1 Rainfall Data Collection

To design an appropriate range of rain intensities leading to post-wildfire erosion and debris flow, in addition to performing a literature review, we gathered real-time rain-gauge data from two

recent California post-wildfire debris flow events. Monterey County and Silverado Canyon debris flow events provided more rain intensity data. In addition, precipitation maps and hourly precipitation summaries for their rain station network were acquired through the California Nevada River Forecast Center (CNRFC and NOAA 2021).

Figure 1.1a shows the hourly rain intensities for the flow in Monterey County, CA, along River Road in the early hours of January 27, 2021. The rain gauge station location was within the River Fire burn scar which burned on August 16, 2020. The debris flow onset correlates with the maximum hourly rainfall intensity of 8.89 mm/hr at 4 a.m. PST on January 27 and 19.8 mm cumulative rainfall up to that time. However, as it began to rain again, the total cumulative rainfall increased to 83.1 mm, but no more mudflows were reported during this time. Figure 1.1b shows the flow data in Silverado Canyon, CA, in the last hour of January 28, 2021. The rain gauge station is within the Bond Fire burn scar, which burned seven days from December 3 – 10, 2020. The maximum hourly rainfall intensity was 12.19 mm/hr at 11 p.m. PST on January 27, and the cumulative rainfall after the storm was 39.4 mm. Despite higher rainfall intensity rates for 15-minute intervals, the average hourly rainfall intensity rates are consistent with the average

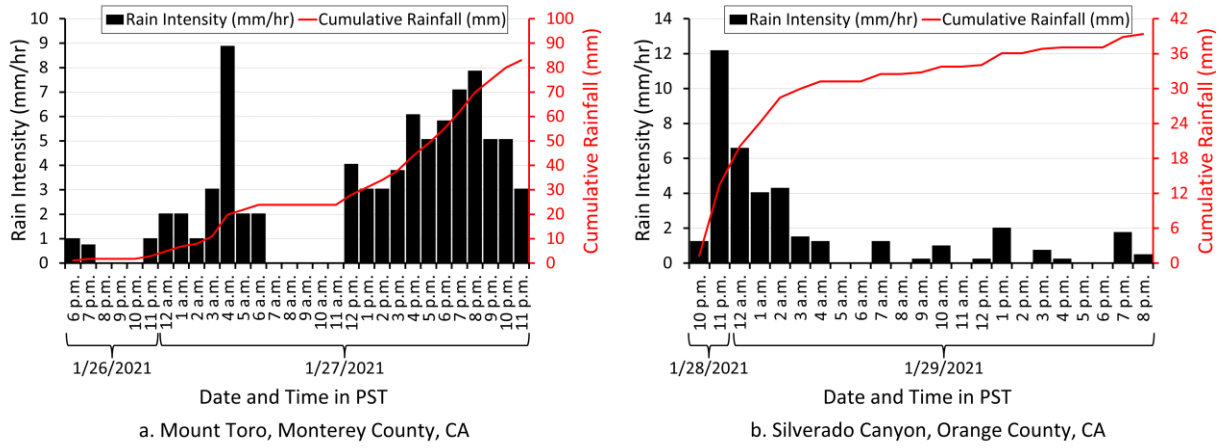

Figure 1.1: Mudflow-triggering rain intensities, January 2021 in California, US: (a) Monterey County, along River Road, (b) Orange County, Silverado Canyon

hourly rates found during this research for various post-wildfire mudflows that occurred in late January of 2021.

1.2.2 Experimental Setup

Experiments are performed outside using a custom-built setup. Figure 1.2 shows a 99.1 cm by 99.1 cm box made of wood and plywood with wheels for easy manipulations. The inner dimensions are 91.4 cm by 76.2 cm, with a 1.9 cm high wood plank that allows the water and superficially eroded material collection. Angled barriers guide sand and water runoff into a catchment at the bottom of the slopes. A zinc-plated slotted angles frame connected with nuts and bolts supports the experiment box and adjusts the slope.

After finding appropriate rain intensity values for storms that triggered post-wildfire mudflows, a suitable rain simulation system is built to reach the target values. Modeling the system based on Carvalho et al. (2014) with adjustments, a 330.2 cm tall supporting frame supports the hose and spray nozzle at the top. Calibration of different spray nozzles and pressures enables the

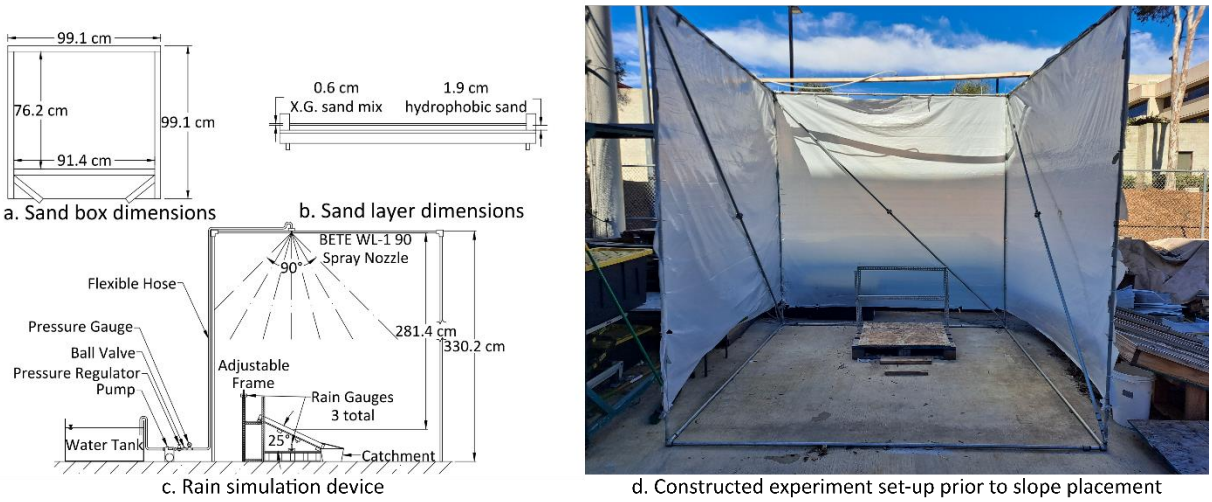

Figure 1.2: Experimental set-up with a sandbox, adjustable frame, eroded material and water catchment, frame to hold the rain nozzle, water tank, water pump with a pressure regulator, and a pressure gauge

physical modeling of the higher rain intensity values for reported events measured within 15-minute intervals, such as the reported 15 mm/hr in the Santa Monica Mountains, CA, and 50 mm/hr in Montecito, CA. For example, at a water pressure of 241.3 kPa, the HH-4.3W nozzle with a 120° spray angle from Spraying Systems Co. gives the lower 15-minute rain intensity of 15 mm/hr with a drop size diameter range of 0.55 – 3 mm and an average drop size diameter of 1.6 mm, and a BETE WL-1 90 nozzle with a 90° spray angle gives a 15-minute rain intensity of 50 mm/hr with the same drop size ranges. The rain intensity is measured with two rain gauges placed on either side of the experiment box and one placed at the top of the adjustable frame during the calibration and later for each experiment.

Coarse, medium, and fine uniform sands are artificially hydrophobized following the procedure outlined by Movasat and Tomac (2020), shown in Table 1.1. The water drop penetration test classifies the sand as severely hydrophobic for each batch. First, the sand is submerged in a 90% RGA 100 alcohol and 10% triethoxy-n-octylsilane solution by volume for 48 hours, mixing the sand after one day immersed. After this, the submerged soil is washed to remove any reactive compounds and oven-dried for 24 hours. For the XG sand mix, the total used mass is 2250 g, adjusted for each experiment, with a maximum of 3% XG and 97% base sand by mass.

Table 1.1: Soil contact angle and particle grading parameters

Soil	Contact angle (°)		Angle of Repose (°)	C_u	C_c	D_{10} (mm)	D_{50} (mm)	D_{60} (mm)
	Hydrophilic	Hydrophobic						
Fine	60	115	30	1.50	0.90	0.15	0.2	0.23
Medium	38	100	32	1.67	1.01	0.28	0.4	0.47
Coarse	27	96	34	1.53	1.03	0.46	0.65	0.70

While on level ground, the hydrophobic sand is uniformly distributed into the sandbox up to a height of 1.9 cm. Different setups investigate an optimal erosion control: (1) control setups with untreated hydrophobic sand, (2) setups with XG and sand mix pluviated over the hydrophobic layer, (3) 24 h cured XG-sand mix that is sprayed with 16.5% concerning the layer's mass, or 371.25 g, of water. Then, the adjustable frame is set at the target angle's height, and the sandbox is rolled over carefully and gently placed at the angle. Achieved sand densities for these experiments were 733 kg/m^3 for coarse, 944 kg/m^3 for medium, and 1020 kg/m^3 for fine.

1.3 RESULTS

First, 50 mm/hr rain intensity experiments without any XG provide the erosion baseline at 10°, 15°, 20°, and 25° slopes for medium sand and 10°, 25°, and 30° for fine sand. Second, we performed raining experiments on sand slopes sprinkled with uncured XG-sand mix. Although this method seemed to aid in erosion resistance at first, the surface layer soon becomes over-wetted during the trial 15 min of rain, and the whole swollen XG layer excessively deforms and fails. Therefore, covering the sand surfaces with an uncured XG-sand layer increases the risk of failure for prolonged rain events. Sprinkling pure XG was originally considered, but indoor, small-scale experiments, seen in Fig. 1.3, with an identical rain simulation device from Carvalho et al. (2014) resulted in the XG-sand mix experiencing less surface morphology (Figure 1.3c) than the pure XG trial with multiple crater-like ridges from the rain drop impacts.

Third, a 0.6 cm of XG mixed with hydrophilic sand layer is placed over hydrophobic sand and wetted. After drying, the XG treated soil layers solidify, like the study conducted by Soldo et al. (2020). Microscopic images of pieces of naturally re-dried crusts with no deformation from each sand type show different styles of XG bonding in each sand. Figure 1.4 shows that in the coarse sand, XG bonds are web-like, with very tiny particles attached to them as the strands span

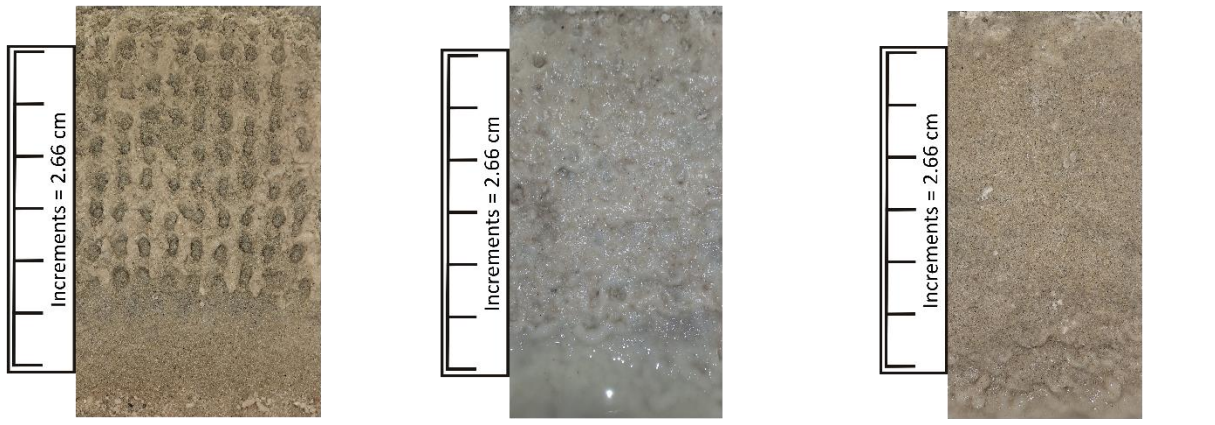

a. Hydrophobic sand b. XG over hydrophobic sand c. XG w/ sand over hydrophobic sand

Figure 1.3: Small-scale trial experiments

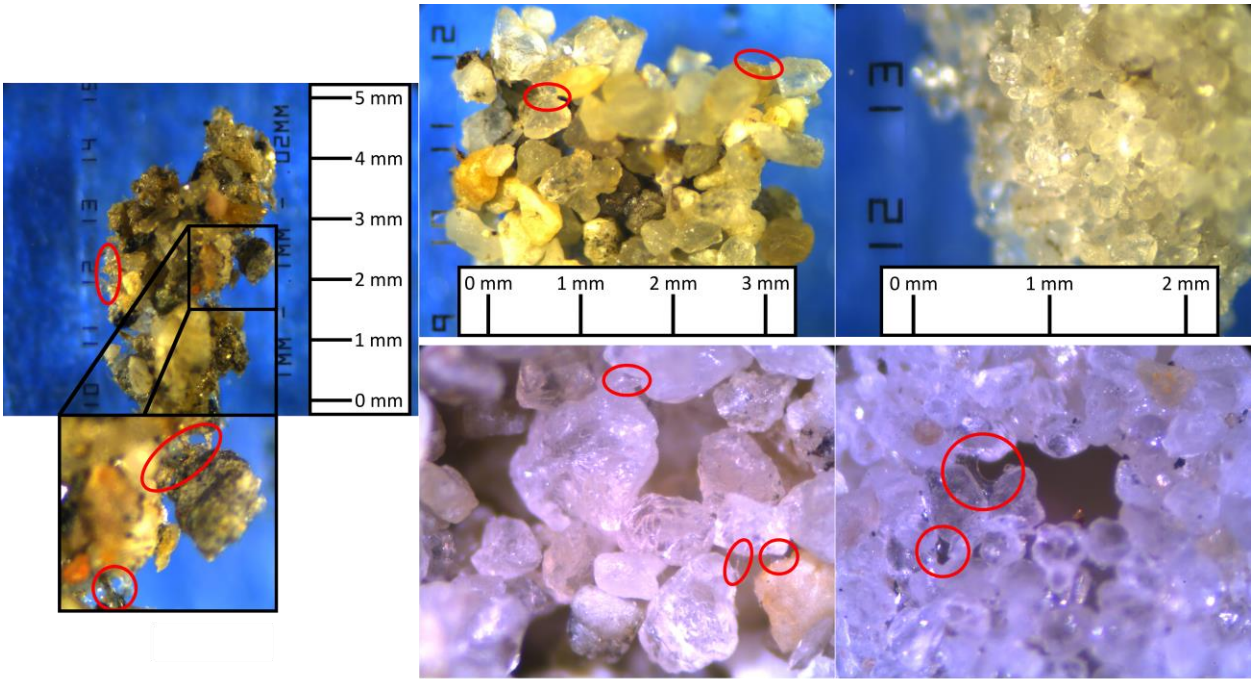

a. Coarse

b. Medium. *Top*: For scale
Bottom: For better bond view

c. Fine. *Top*: For scale
Bottom: For better bond view

Figure 1.4: Microscopic images of cured 3% XG crust bonds in the three sand types: (a) coarse, (b) medium and (c) fine sand

from a large particle to another. The bonds encapsulate the particles completely in the fine sand, almost sheet-like, as seen in Fig. 1.4c. The medium sand crust bonds seem to be, qualitatively, a combination of the other two-crust bonds, with pure XG strands spanning from particle to particle and some more meaningful bonds between particles from direct contact with each other.

1.3.1 Surface Morphology

Overall, experiments reveal full and partial surficial erosion at different rain intensities, slopes, and sand types, with a majority successfully reducing erosion, some examples can be seen in Figure 1.5. Furthermore, some experiments with XG erosion control behave unfavorably and gradually develop surface morphologies that enhance erosion or water overflow. Figure 1.6 classifies surface erosion morphology types into six different scenarios identified from all the experiments, with closer views shown in Figures 1.7, 1.8, and 1.9. Tables 1.2 and 1.3 summarize experimental results and erosion types, including those without visible surficial changes. For example, Figure 1.6a shows rain erosion of untreated hydrophobic medium sand at a 15° slope. The sand surface slowly erodes under the raindrop's impact, and the erosion subsequently increases. Similar behavior occurs at the 10° and 15° medium, and 10° for fine sand slopes under higher rain intensity. Furthermore, the erosion of the untreated slope evolves into channels, as seen

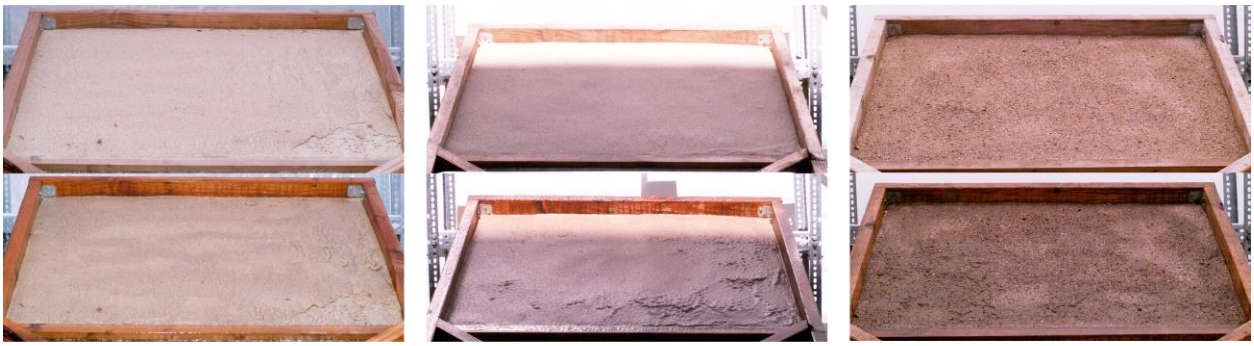

a. Medium 3% XG not cured, one day after first raining experiment. *Top*: Before *Bottom*: After

b. Medium 1% XG cured. *Top*: Before *Bottom*: After

c. Coarse 2% XG cured. *Top*: Before *Bottom*: After

Figure 1.5: Examples of successful experiments at 50 mm/hr rain intensities and 25°, before and after

in Fig. 6b, at 20° and 25° slopes.

Slopes treated with XG exhibit either stability or erosion at more minor scales than untreated slopes, or surface plastic deformation. Two instances of an extreme surface morphology occur in an uncured mix of 0.5% XG and medium sand at the 20° and 25° angles, seen in Figure 1.6c. First, large horizontal sections slide down as the uncured mix had no solidified bonds while containing little XG. Subsequently, the exposed hydrophobic sand develops channels like the untreated slopes at these same angles. By increasing the concentration of XG in the mix with medium sand, for example, to 3%, the horizontal erosion effect persists, but at a significantly smaller scale without channels (Figure 1.6d).

Figure 1.6e shows sliding ridges observed with various XG percentages in the sand and sprinkled with water cured for 24 hours. The curing process produces a crust with solid bonds between the particles (Figure 1.4) and less erosion. As a result, small ridges form under raindrops impact in different surface sections that then attempt to slide down while the rest of the crust holds in place. While cured, coarse sand slopes with a mix of 2% and 3% XG at 25°, medium sand experiments with 1% XG at 25° and 3% XG at 15° and 20°, and fine sand slopes with 3%

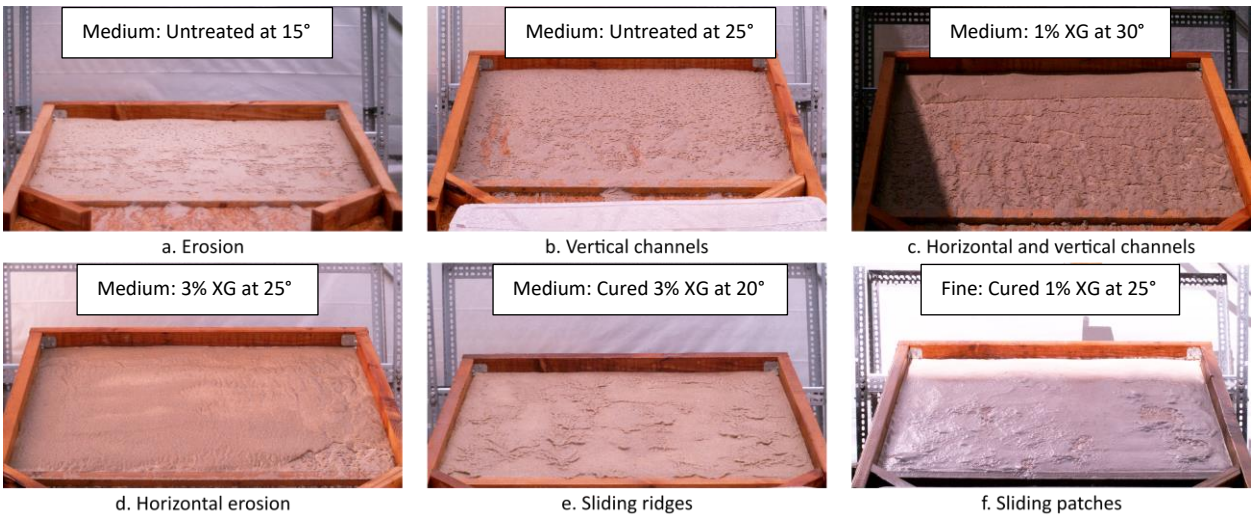

Figure 1.6: Observed erosion types

a. Erosion

b. Vertical channels

Figure 1.7: Detail views of Figure 1.6a and Figure 1.6b

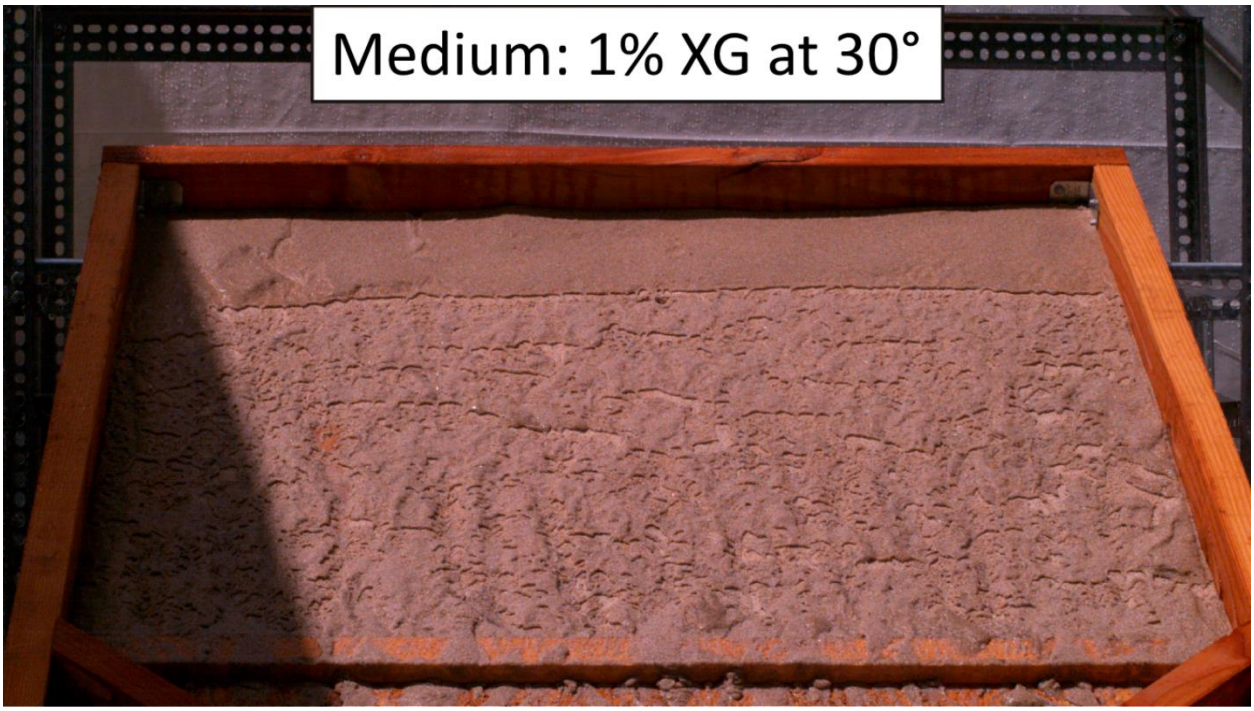

c. Horizontal and vertical channels

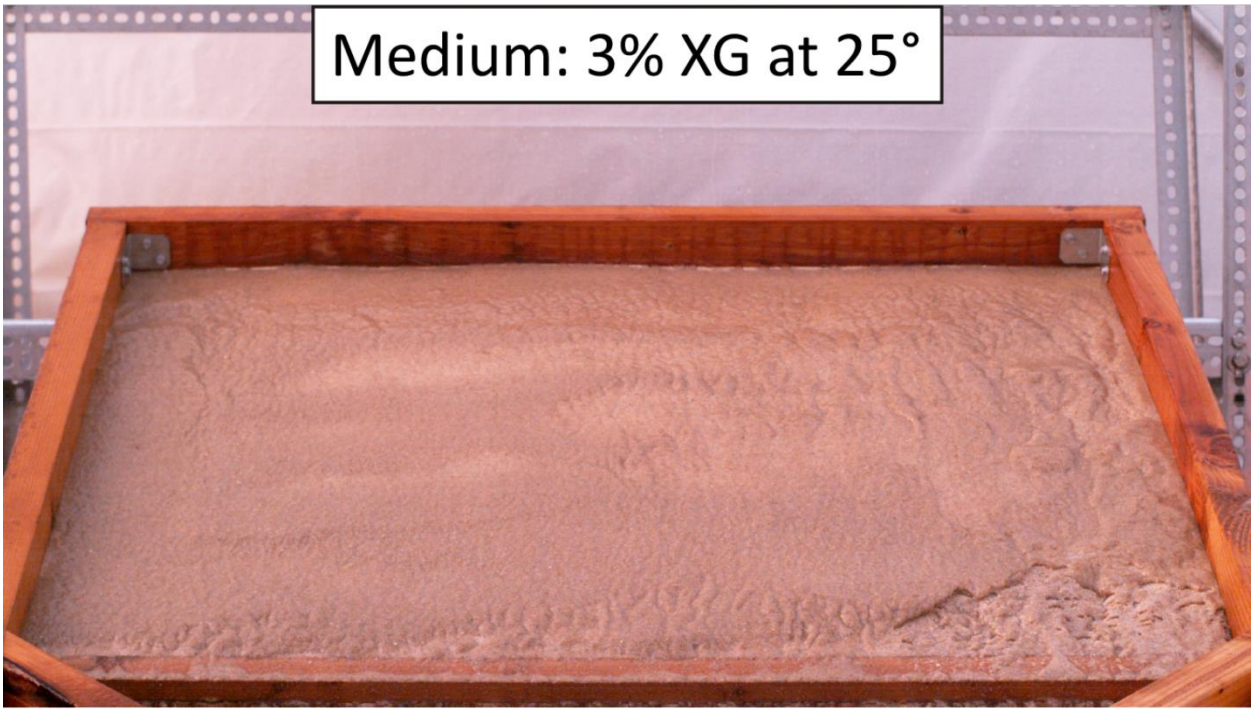

d. Horizontal erosion

Figure 1.8: Detail views of Figure 1.6c and Figure 1.6d

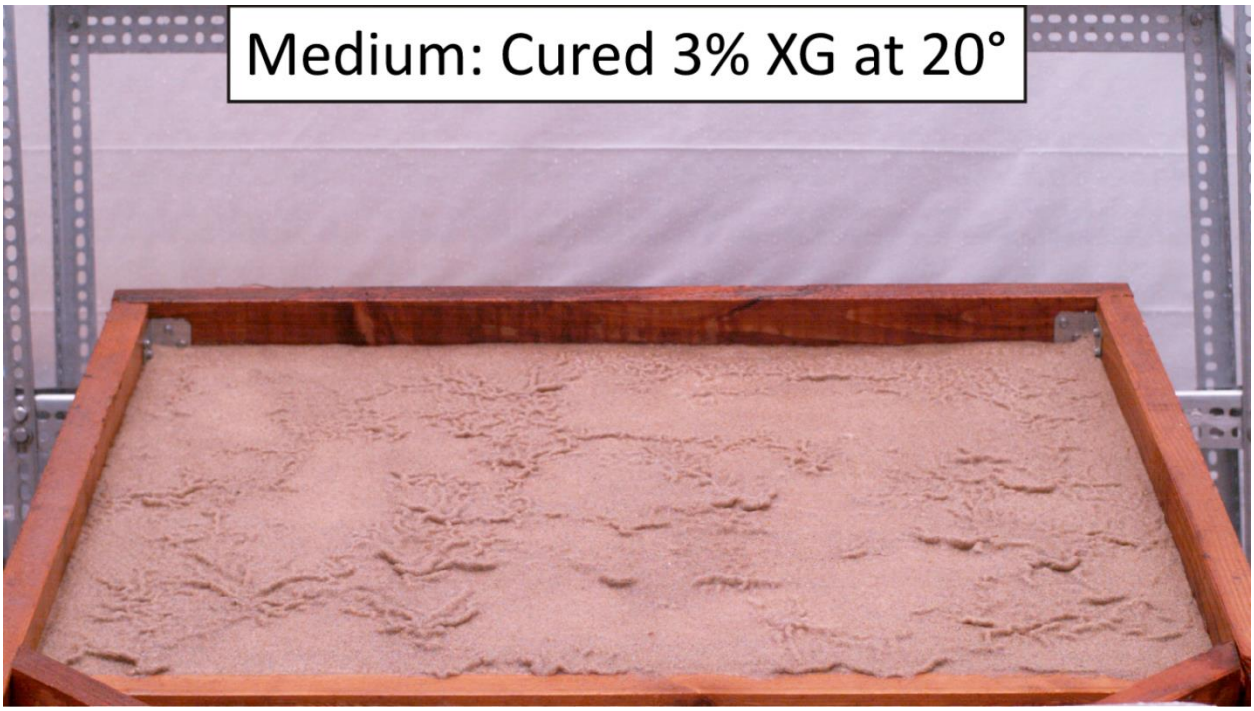

e. Sliding ridges

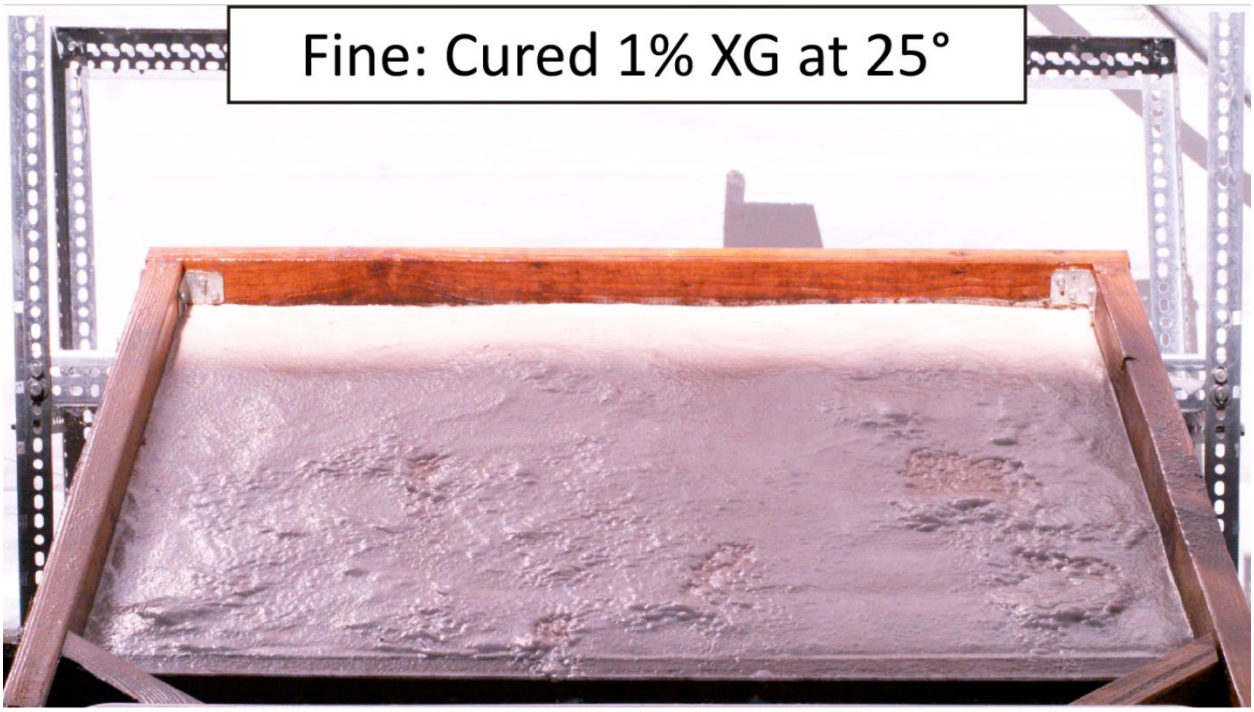

f. Sliding patches

Figure 1.9: Detail views of Figure 1.6e and Figure 1.6f

Table 1.2: Surface erosion type and runoff data for each cured experiment with rain intensities of 50 mm/hr for 15 min

Tests	XG %	Test Type	Surface Erosion Type	Normalized Runoff Water (mL/cm^2)	Normalized Runoff Soil (mg/cm^2)	% Eroded
10°						
Fine	0	N	Erosion	1.14	46.05	2.52
	3	C	None[a]	1.62	0	0
Medium	0	N	Erosion	1.06	37.31	2.42
15°						
Medium	0	N	Erosion[c]	0.16	78.45	4.68
	3	C	Sliding ridges[a]	1.15	0.3	0.01
20°						
Fine	3	C	Sliding ridges[a]	0.02	0.0004	0.02
Medium	0	N	V channels	0.26	73.31	3.84
	0.5	N	H+V channels	0.73	376.33	14.79
	3	C	Sliding ridges[a,c]	1.15	0.32	0.01
Coarse	3	C	None[a]	0.23	0.64	0.02
25°						
Fine	0	N	V channels	0.69	325.26	16.59
	1	C	Sliding patches[a,c]	0.62	1.327	0.05
	2	C	Sliding patches[a]	0.74	229.93	8.86
	3	C	Sliding ridges[a]	0.1	0.95	0.03
Medium	0	N	V channels[c]	0.59	57.96	3.46
	3	N	H erosion[c]	0.35	69.99	2.1
	3	ND	Sliding patches[a,b]	0.64	1.58	0.05
	1	C	Sliding ridges[a,b]	0.4	0	0
	3	C	Sliding patches[a]	0.23	1.27	0.04
Coarse	2	C	Sliding ridges[a,b]	0.26	0.12	0.01
	3	C	Sliding ridges[a]	0.26	0	0
30°						
Fine	0	N	V channels	0.6	1446.08	65.83
Medium	0.5	N	H+V channels[c]	0.79	531.97	21.82

Note: N = not cured; ND = one day after corresponding N test; C = 24h cured.; V = Vertical; H = Horizontal
[a]Successful in reducing erosion compared to untreated hydrophobic slopes
[b]Shown in Figure 1.5
[c]Used as reference picture in Figure 1.6

Table 1.3: Surface erosion type and runoff data for each cured experiment with rain intensities of 15 mm/hr

Tests	XG %	Rain Duration (min)	Surface Erosion Type	Normalized Runoff Water (mL/cm^2)	Normalized Runoff Soil (mg/cm^2)	% Eroded
25°						
Fine	1	15	Sliding ridges	0.02	0	0
	1	30	Sliding ridges	0.07	0	0
	3	15	Sliding ridges	0.24	0	0
	3	30	Sliding ridges	0.38	0.002	0.06
Medium	1	15	Sliding ridges	0.14	0	0
	1	30	Erosion	0.29	0.002	0.09
	3	15	Sliding ridges	0.04	0	0
	3	30	Sliding patches	0.05	0	0
Coarse	3	15	Sliding ridges	0.24	0	0
	3	30	Sliding ridges	0.54	0	0

Note: All experiments were successful with little to no erosion

XG at 20° and 25° all experienced the morphology type in Figure 1.6e. Figure 1.6f shows a morphology characterized by individual sliding patches formed when the bonds from the cured XG were not strong enough to hold the sliding sections in place. For example, individual sliding patches occur in the medium sand with a mix of 3% XG at the 20° to 25° slopes and fine sand with 1 and 2% XG at a 25° slope, while 3% XG prevents sliding patches of fine sand. In addition, while the not cured mix of 3% XG develops horizontal erosion when allowed to cure by re-drying and to test again the day after, a tiny sliding section develops.

In addition, Table 1.3 summarizes observations of surface morphology at a lower rain intensity of 15 mm/hr, which overall show more favorable results. Coarse and fine sands with different cured XG percentage mixes formed small ridges after 15 minutes, with little to no changes after another 15 minutes. For cured medium sand, both 1% and 3% develop very few ridges after 15 min, but after another 15 min, another surface erosion type occurs, where a small patch begins to slide down the slope for the mix of 1% XG. Furthermore, at this lower rain intensity, an uncured

mix of 0.5% XG does not develop the extreme horizontal erosion and channels, but only the horizontal erosion at the smaller scale, much like the uncured 3% XG at the higher intensity.

1.3.2 Effects of Sand Type, XG Content, and Slope Angle on Erosion Susceptibility and Water Runoff

1.3.2.1 Sand erosion

The amounts of collected sand normalized by the experiment surface area are plotted against the XG percentage in the mix and the slope angle in Figures 1.10 and 1.11 to understand erosion better. The overall trend indicates that XG percentage increase better stabilizes slopes, and more XG is needed at higher angles and finer sands. Furthermore, erosion susceptibility in treated fine sands is problematic due to the random development of unfavorable surface morphologies. For example, Figure 1.10a shows that although most experiments at 1% to 3% XG-sand mix cured for 24 hours develop different levels of sliding ridges, the measured erosion is still significantly reduced compared to the pure hydrophobic sand experiments. However, fine sand with 24 h cured

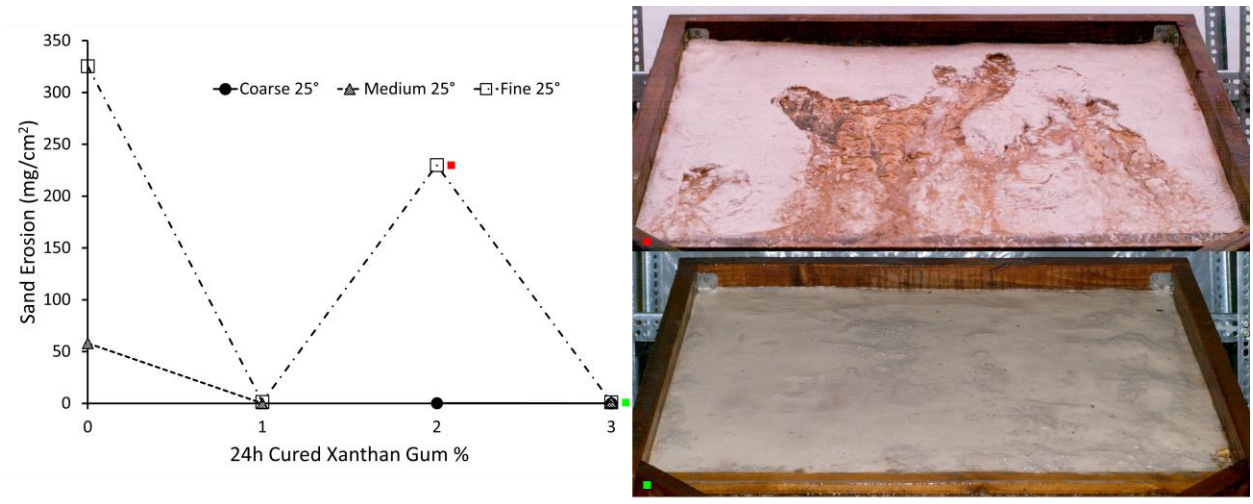

a. Corresponding symbol and colors for reference image data points

b. 24h cured fine sand at 25°. *Top:* 2% XG *Bottom:* 3% XG

Figure 1.10: Sand erosion vs. the cured XG-sand mix for varying slope angles for 50 mm/hr rain intensities

2% XG at 25° performs poorly (Figure 1.10b). Top Figure 1.10b shows how the cured protective layer above the pure hydrophobic sand is being compromised as a piece of the crust breaks away. The water that continuously rains and flows down the slope chips away pieces at the exposed location, increasing the size of the sliding patches.

From the slope angle perspective, slopes above 20° angle enhance erosion in cured XG-sand, including for all fine sands regardless of the XG percentage, and medium sand with 3% XG. Furthermore, interesting connections exist between the observed surface morphology and erosion rates. For the coarse sand, the sand runoff at a 20° slope was 0.64 mg/cm^2, while the 25° slope yielded no collected erosion. The 20° coarse slope experienced no unusual surface morphology, while the zero-erosion 25° slope formed ridges (Table 1.2). Unlike a whole section pulling down and forming ridges, tiny particles broke their XG bonds and slid down the slope, leading to no sliding ridge formation. Also, while the collected erosion was higher at the 20° than 25° slope, it was only 4.16 g, an amount of no concern. The same phenomenon is seen with medium sand at a 25° angle using a mix of 1% XG, with the surface forming sliding ridges and collecting no erosion. Figure 1.11b also shows that the medium and fine sands follow a parallel trend, increasing the collected sand runoff by 0.95 mg/cm^2 when changing the slope from 20° to 25°, also connected to the surface morphology illustrated with Figure 1.11b. Many sliding ridges formed on the medium

a. 24h cured 3% XG coarse sand.
Top: 20° *Bottom:* 25°

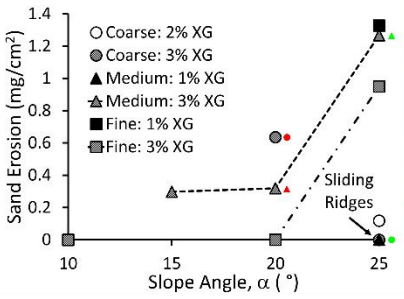

b. Corresponding symbols and colors for reference image data points

c. 24h cured 3% XG medium sand.
Top: 20° *Bottom:* 25°

Figure 1.11: Sand erosion vs. slope angle for 24h cured XG percentages for 50 mm/hr rain intensities

sand experiment with less erosion than coarse sand. The surface morphology changed at the same angle that the coarse sand experienced a change from sliding ridges to sliding patches. Though fine sand did develop ridges throughout most of its surface, a tiny patch eroded at the bottom right of the slope.

Ridge development allows less sand runoff because sand particles that roll downhill now have a stronger cohesive force from the cured XG. However, after continued rain at high intensities, the stronger crust bonds turn from solids to gooey, and the ridges run the risk of evolving into sliding patches. Based on this, curing a sand mix with 3% XG and developing ridges decreases the amount of sand runoff but can lead to sliding patches and elevated erosion.

1.3.2.2 Water runoff

Figure 1.12a shows conclusive results at highest slopes of 25° for all sand types and percentages of XG, and relatively inconclusive results at less steep angles. At 25° and cured 3% XG sand mix, the water runoff is highest over coarse, then medium, and then fine sand slopes.

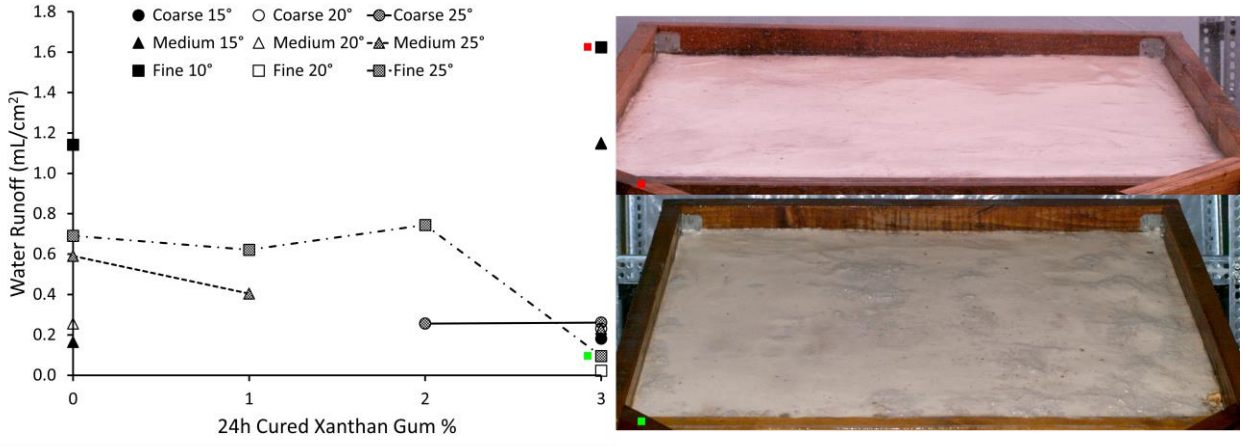

a. Corresponding symbol and colors for reference image data points

b. 24h cured 3% XG fine sand. *Top:* 10° *Bottom:* 25°

Figure 1.12: Water runoff v. 24h cured XG percentage for varying slope angles

The water runoff remains roughly the same at untreated to 1% XG as the surfaces formed vertical channels and sliding patches. Furthermore, the water runoff slightly increases at 2% XG as the surface develops larger sliding patches. Finally, the water runoff decreases sharply between 2% to 3% XG for fine sand once the surface forms small sliding ridges. Figure 1.12b also shows the difference in surface morphology between the fine sand slopes with 3% XG at 25°. The 10° slope at the top of Figure 1.12b has no surface morphology changes and yielded a much higher water runoff, while the 25° slope has small sliding ridges and experienced a reduced water runoff.

Figure 1.13 shows an inverse relationship between the water runoff and the sand erosion for slopes covered with medium cured 3% XG-sand mix. When the medium sand erosion is lower for the shallower slopes, around 0.3 mg/cm^2, the water runoff is 1.15 mL/cm^2. However, once the medium sand erosion increases to 0.95 mg/cm^2, the water runoff significantly decreases to 0.23 mL/cm^2.

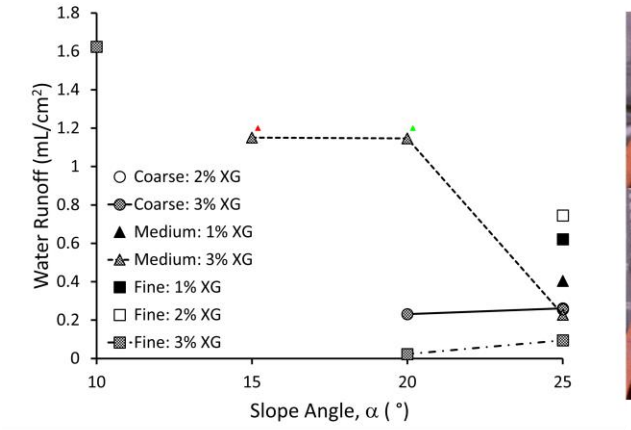

a. Corresponding symbol and colors for reference image data points

b. 24h cured 3% XG medium sand. *Top:* 15° *Bottom:* 20°

Figure 1.13: Water runoff v. slope angle for varying 24h cured XG percentages

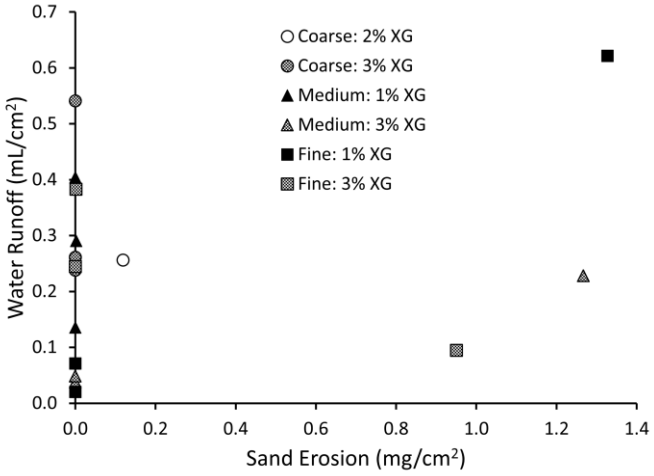

Figure 1.14: Water runoff v. sand runoff for 24h cured XG percentages at a 25° angle

Coarse and fine sand experiments show a slight water runoff increase with an increasing slope, regardless of sand erosion. This idea is depicted in Figure 1.14, which when looking at a 25° slope, there were coarse, medium, and fine sand trials with cured XG percentages where there was no or little erosion and a water runoff range of 0.02 mL/cm^2 to 0.73 mL/cm^2. A majority of these no erosion data points are below 0.30 mL/cm^2. To conclude, although the water runoff can be high without erosion, both water and sand runoff increase exponentially once the erosion starts.

1.3.3 Rain Intensity Effect

Figure 1.15 shows the sand and water erosion trends, as the rain intensity increases from 15 mm/hr to 50 mm/hr at the steepest slope of 25°. The tested XG percentages for each sand show no sand erosion at 15 mm/hr low rain intensity (Figure 1.15a, Table 1.3). At the higher rain intensity of 50 mm/hr, 3% XG controls erosion better than their 1% counterparts overall, except for the experiment in medium sand. Furthermore, 3% XG overall shows less water runoff sensitivity to rain intensity, although there are some variations between sands (Figure 1.15b). Interestingly, cured fine sand with 1% XG has the lowest water runoff at lower rain intensities but

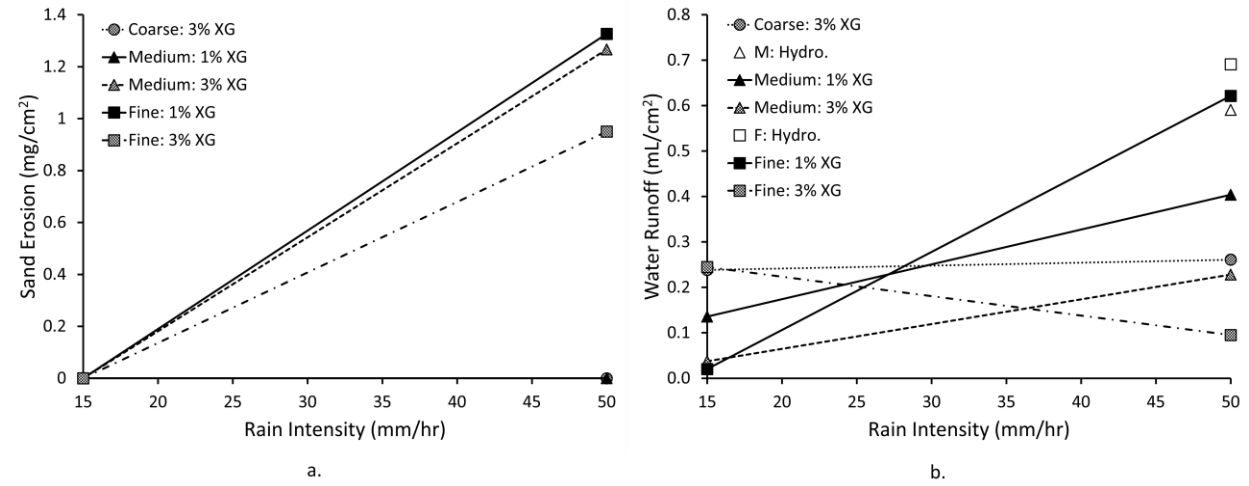

Figure 1.15: (a) Sand runoff v. rain intensity at a 25° angle, (b) water runoff v. rain intensity at a 25° angle

increases the most as the rain intensity increases, shown in Figure 1.15b, indicating high erosion potential to turn catastrophic in fine sands, even when improved with XG. Finally, cured coarse sand with 3% XG is relatively insensitive to rain intensity.

Time of raining changes surface morphology, erosion, and water runoff. Looking at Figure 1.16, at the lower intensity of 20 mm/hr, there was no erosion collected after the initial 15 minutes, but between 15 and 30 minutes, there was erosion and some sliding patch failures in both the 1% medium and the 3% fine, but the 1% fine and 3% coarse and medium continued to work during this raining time. Figure 1.16b shows an example of how the surface morphology could change as the rain duration increases. The example shows that the erosion stems from the developed ridge, even though it is small. Much like seen in the previous section, when the surface morphology type changes from ridges to another kind, there is an increase in sand runoff. On the contrary, Figure 1.17 shows that the water runoff for the lower rain intensity of 15 mm/hr stayed consistent with little change in slopes for the duration of the experiment. The higher the XG percentage, the lower the water runoff for cured medium sand. For cured fine sand, the higher the XG percentage, the

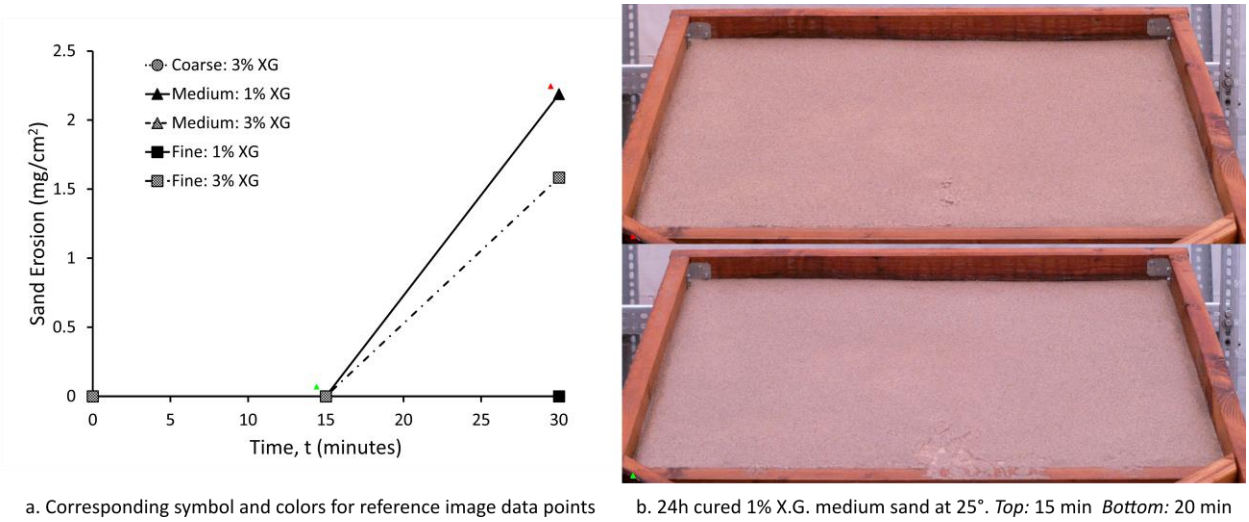

a. Corresponding symbol and colors for reference image data points

b. 24h cured 1% X.G. medium sand at 25°. *Top:* 15 min *Bottom:* 20 min

Figure 1.16: Sand runoff v. time for rain intensities of 15 mm/hr at a 25° angle

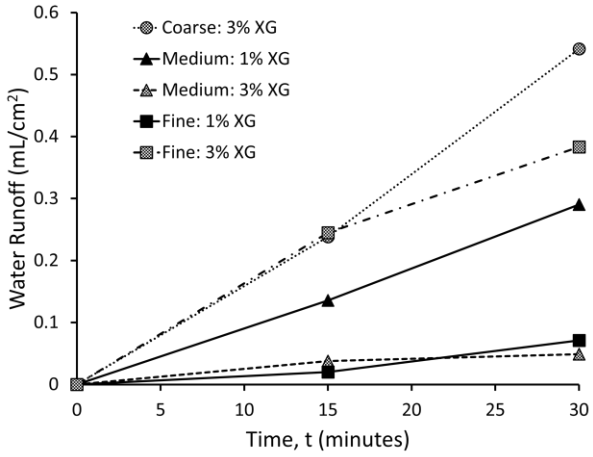

Figure 1.17: Water runoff v. time for rain intensities of 15 mm/hr at a 25° angle

higher the water runoff, and the most water runoff comes from cured coarse sand with 3% XG.

1.4 CONCLUSIONS

Wildfire frequency has been increasing in recent years, posing more threats to the environment, people, and civil infrastructure not only because of burning but also post-wildfire mudflows. Burned scars are more susceptible to mudflows, and debris flows when rain falls onto slopes that lost vegetation and whose surficial soil layers turned hydrophobic. This paper explores the advantages and limitations of surficial soil improvement of burned scars with biopolymer, specifically xanthan gum (XG), using various slopes at high and low rain intensities. However, this controlled laboratory study does not upscale specific findings to natural slopes with varying inclinations and heterogeneous surficial hydrophobicity.

This study concludes that, despite the limited available literature, sprinkling surfaces with pure XG does not yield sufficient stability against erosion for prolonged rains. Furthermore, a different technique is proposed that pre-mixes XG and sand in a dry state and then spreads and wets the mix over hydrophobic slopes. The erosion values for each cured experiment are significantly reduced compared to the untreated hydrophobic slopes. Furthermore, this study shows that curing the pluviated sand and XG mix for a day after wetting decreases the sand runoff and keeps the water runoff relatively low. However, we classify the surface morphology of treated slopes after the low and high-intensity rain and identify possible pitfalls. Specifically, fine, medium, and coarse severely hydrophobic sand, 10° to 30° sloped surfaces, covered with a layer of XG-sand mix at 1% to 3% mass ratios, are tested under 15 mm/hr and 50 mm/hr rain intensities. The sand mixed with XG was untreated, thus not hydrophobic. Sand coarseness plays a significant role in XG erosion control. Low rain intensity 15 mm/hr does not erode slopes with 1% to 3%

cured XG mixes across a variety of slopes from 10° to 25°, although minor erosion occurs in medium and fine sands for 1% XG mix.

Furthermore, at high 50 mm/hr rain intensity, coarse sands perform well at all inclinations when treated with 3% XG and show only a small amount of erosion with 2% XG. Medium sands, on the contrary, are more sensitive, and although 3% XG performed well at wide slope ranges from 15° to 25°, extreme erosion occurs when the XG percentage was as low as 0.5% at higher angles of 20° and 30°. The transition of medium sand occurs at 25°, where small erosion patches form. Fine sand covered with 3% XG mix performs well at angles 10° to 25°, where small ridges form at steeper slopes. Furthermore, lower 1% and 2% XG fine sand mixes perform poorly at 25°.

Despite surficial improvements, the water runoff can be high without erosion, indicating limited infiltration capabilities. In addition, both water and sand runoff increase exponentially once the erosion starts. It is essential to consider the expectancy of the rain because this study shows modified surface morphology formed during the rain event. Some experiments show the development of ridges that can further erode during rain.

Finally, this study recommends practical XG percentage of the mix for slopes improvement, relying on results at 25° angle. The surface erosion types were similar for coarse and medium sand, making 2% XG the most material-efficient while having negligible erosion with the same water runoff seen with 3% XG. Finally, for fine sand, 1% XG has a high likelihood of forming a larger sliding patch the more prolonged the rain duration, so ≥3% XG is recommended.

Acknowledgements

Chapter 1, in part, has been submitted for publication of the material as it may appear in Journal of Geotechnical and Geoenvironmental Engineering, Chavez De Rosas, Jonathon; Tomac, Ingrid, 2022. The thesis author was the primary researcher and author of this paper.

CHAPTER 2: PERFORMANCE OF XANTHAN GUM AS POST-WILDFIRE MUDFLOW MITIGATION UNDER NATURAL ENVIRONMENT CONDITIONS

2.1 INTRODUCTION

While the experiments from Chapter 1 provided a wide variety of data on the effectiveness of xanthan gum mixed with sand on a controlled slope with high rain intensities, the performance of these treatment types exposed to a natural environment is as pertinent to fully understanding the mitigation technique. Therefore, larger semi-permanent slopes were built and were exposed to environmental conditions for 6 months. Throughout the duration of the experiments, untreated and treated hydrophobic slopes were exposed to tree debris, animal interactions, and natural rainfall, yielding interesting data.

2.2 METHODOLOGY

For the same three types of sand from Chapter 1 referred to as coarse, medium, and fine, shown again in Table 2.1, two angles were studied and compared to their untreated counterparts.

2.2.1 Experiment Preparation

A total of six slope beds were created out of wood, two beds for each sand type angled at 17° and 21°. Each bed was made to have two flumes with inner dimensions of 43.8 cm width and

Table 2.1: Soil contact angle and particle grading parameters.

Soil	Contact angle (°)		Angle of Repose (°)	C_u	C_c	D_{10} (mm)	D_{50} (mm)	D_{60} (mm)
	Hydrophilic	Hydrophobic						
Fine	60	115	30	1.50	0.90	0.15	0.2	0.23
Medium	38	100	32	1.67	1.01	0.28	0.4	0.47
Coarse	27	96	34	1.53	1.03	0.46	0.65	0.70

182.9 cm in length. Measuring through critical surface tension, Huffman, et al., (2001) found soil hydrophobicity to be stronger at the surface and dissipate as the depth increases, with the last relevant depth further analyzed being 6 cm. According to these findings, the flumes were then pluviated, seen in Figure 2.1a, with the sand layers seen in Figure 2.1b to mimic a similar effect of the soil depths using coarse, medium, and fine uniform sands are artificially hydrophobized following the procedure outlined by Movasat and Tomac, (2020), previously outlined in detail in section 1.2.2. A roller system and wheel guides with a horizontal support system allowing sliding ability were created to keep a constant drop height while pluviating the sands. The bottom of the slopes contained a wood barrier to support the bottom layers while allowing the top layers with hydrophobicity and the XG treatment to be collected in a catchment for erosion and water overflow measurements after rain events.

The left flume on each slope bed contained unmitigated hydrophobic sand while the right flumes had the XG treatment. The initial treatment of the slopes had 0.5% concentration by mass

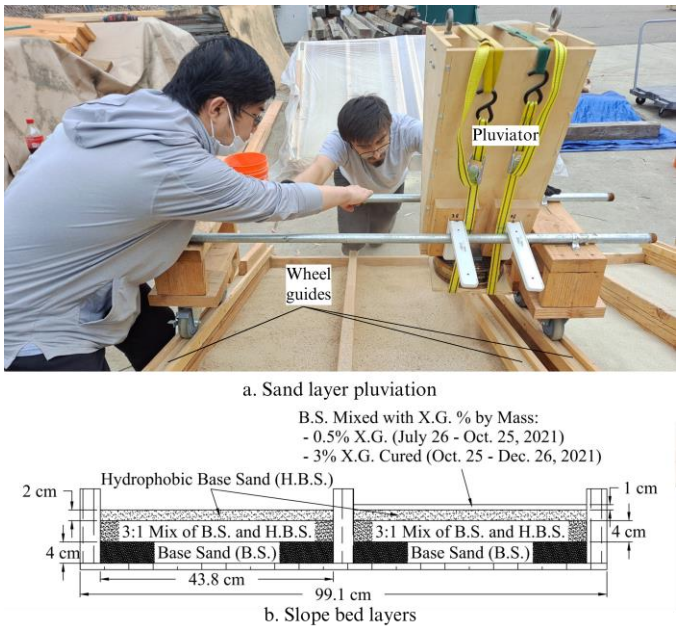

Figure 2.1: Experiment preparation and layers

of XG mixed with the base sand. The first seven rain events used this percentage. On November 21, 2021, the treated slopes were re-covered using 3% concentration by mass of XG mixed with the base sand and cured immediately after by spraying the layer with 16.5% by mass of water, forming a hardened crust layer after drying. Achieved sand densities for these experiments were 1092 kg/m^3 for coarse, 1365 kg/m^3 for medium, and 1638 kg/m^3 for fine.

2.3 RESULTS

Initially, the hydrophobic base sand on the right flume of each slope bed was covered with 1 cm of the base sand mixed with 0.5% XG (Figure 2.2). Throughout the experiment, leaves, twigs, and bark from the surrounding trees landed on the slopes, as well as a family of raccoons occasionally stepping on the slopes. With all these external factors commonly occurring in nature, these experiments paired with natural rain events (RE) provide results for real-world performance of hydrophobic slopes post-treatment for coarse, medium, and fine sand. Table 2.2 summarizes the nine REs occurring over the span of July 26, 2021, to December 26, 2021, with data courtesy of

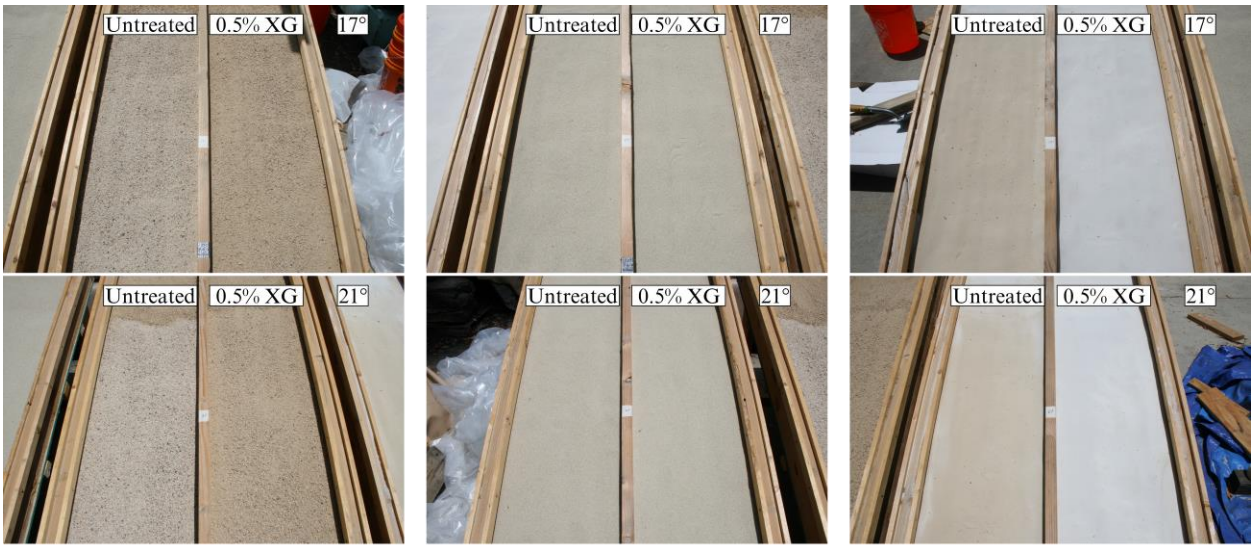

Figure 2.2: Slope beds after placement

Table 2.2: Data and slope treatment type for each rain event courtesy of MesoWest from the University of Utah (https://mesowest.utah.edu/)

RE	Date	Station ID	Duration (min)	Avg. *i* (mm/hr)	Max. *i* Time (PST)	Max. *i* (mm/hr)	Treatment Type
1	7/26/2021	E3170	75	0.76	04:45 – 05:00	2.03	U
2	8/11/2021	E3170	31	0.49	04:00 – 04:31	0.49	U
3	9/9/2021	E3170	29	5.78	20:02 – 20:17	9.14	U
4	9/27/2021	E3170	464	0.29	06:01 – 06:15	1.09	U
5	10/5/2021	F8273	435	1.40	01:31 – 01:46	4.06	U
6	10/8/2021	F8273	225	1.02	04:46 – 05:01	3.05	U
7	10/25/2021	F8273	151	1.69	16:31 – 16:46	11.18	U
8	12/14/2021	E3170	750	2.84	12:00 – 12:15	14.22	C
9	12/26/2021	E3170	166	1.52	02:31 – 02:45	14.15	C

Note: RE = rain event; *i* = rain intensity; U = uncured 0.5% XG; C = cured 3% XG

MesoWest from the University of Utah (https://mesowest.utah.edu/). Stations E3170 and F8273 are located 1.85 km and 3.27 km, respectively, from the experiment locations. Table 2.3 contains the erosion and water runoff normalized by the projected surface area for each slope, sand type, and RE.

2.3.1 Surface Morphology Throughout Rain Events

The first two REs did not cause significant changes to the slopes as the rain durations were short and the rain intensities were low. Although uncured when originally applied, the initial rain from RE 1 wetted the XG coating the sand particles and formed a hardened crust layer after drying, much like the cured treatment process that was applied after the seventh RE. After RE 2, raccoons walked along the surface of two slopes, the treated coarse and the untreated fine slopes, both at 17°. The treated coarse sand was not largely affected, but the untreated fine sand contained a section of the hydrophobic layer that was displaced and exposed the less hydrophobic layer beneath. This did not affect the overall trends of the erosion, however, as the 17° fine slopes data in Table 2.3 reveal that the 0.5% XG flume still experienced higher erosion than its untreated

Table 2.3: Normalized erosion and water runoff values for each sand type, angle, and treatment type after rain events

			Coarse				Medium				Fine			
			17°		21°		17°		21°		17°		21°	
	RE	TT	w/o XG	w/ XG%	w/o XG	w/ XG%	w/o XG	w/ XG%	w/o XG	w/ XG%	w/o XG	w/ XG%	w/o XG	w/ XG%
Erosion (mg/cm^2)	1	Uncured 0.5% XG	0.42	0.45	0.59	0.55	0.61	0.39	1.23	1.30	0.68	0.83	0.94	0.85
	2		0.18	0.05	0.12	0.09	0.12	0.05	0.40	0.09	0.28	0.22	0.32	0.26
	3		6.38	2.11	2.95	5.60	97.63	69.16	49.33	31.79	216.82	219.34	293.37	339.71
	4		0.44	0.07	0.13	0.02	0.94	0.30	0.37	0.37	2.12	0.42	1.20	0.90
	5		3.79	5.99	1.79	4.94	5.50	56.31	5.71	77.61	46.21	140.46	58.72	64.26
	6		1.36	0.76	0.21	0.48	0.70	0.86	0.77	2.20	0.90	1.21	1.54	1.75
	7		1.08	0.84	1.14	0.35	3.37	11.95	3.26	20.01	88.05	67.62	114.23	95.16
	8	Cured 3% XG	1.33	1.10	2.19	1.92	6.65	15.48	8.50	12.41	120.31	28.31	34.63	32.84
	9		3.85	1.85	2.19	6.11	6.65	129.65	6.66	93.06	75.95	196.58	86.47	209.98
Water runoff (mL/cm^2)	3	Uncured 0.5% XG	10.33	44.86	22.26	90.59	14.87	35.79	44.77	234.86	37.05	46.62	73.31	80.90
	4		2.15	5.41	0.36	0.56	0.33	0.89	0.61	0.36	0.59	0.57	0.60	0.05
	5		31.86	97.20	21.72	112.51	0.68	138.86	139.84	681.79	14.37	52.42	99.49	131.44
	6		0	0	0.07	0	0	0	0	6.11	0	0	0	0.01
	7		3.44	0.24	2.36	0.24	8.34	11.59	106.30	56.03	40.07	18.65	80.90	23.30
	8	Cured 3% XG	703.40	408.78	15.71	735.20	132.82	1341.02	94.52	1160.67	457.17	307.22	820.82	306.60
	9		25.71	430.20	46.08	474.43	44.36	1348.33	111.54	1142.87	95.01	1004.06	131.44	1004.36

Note: RE = rain event; TT = treatment type; All values are normalized against the projected slope surface

counterpart during RE 3 and the treated coarse sand had less erosion.

RE 3 with a max. 15-min rain intensity of 9.14 mm/hr caused the first significant change in surface morphology, leading to a larger erosion yield for each slope and sand type. Figures 2.3a, 2.3b, and 2.3c depict the increase in surface morphology when comparing the sand types, with the least change being in the coarse slopes, some channels beginning to form on the medium slopes, and deep channels already formed on the fine slopes. As the rain events continued, the channels seen in the fine sand slopes became more prevalent, with extremely large channels (Figure 2.4a). With a cured layer from the XG after continuous raining, more raccoon activity broke apart the surface layer and created more drastic surface conditions exposing the hydrophobic layers susceptible to mudflows (Figure 2.4b).

Concurrent experiments with simulated rainfall had shown that a cured 3% XG-sand mix greatly reduced erosion at rain intensities of 15 and 50 mm/hr, so the performance of this solution when pluviated from above onto eroded slopes was tested for real-world applications (Figures 2.5 and 2.6). Comparing these images prior to re-covering with their corresponding surface

a. Coarse sand b. Medium sand c. Fine sand

Figure 2.3: Surface morphology after RE 3 on September 10, 2021

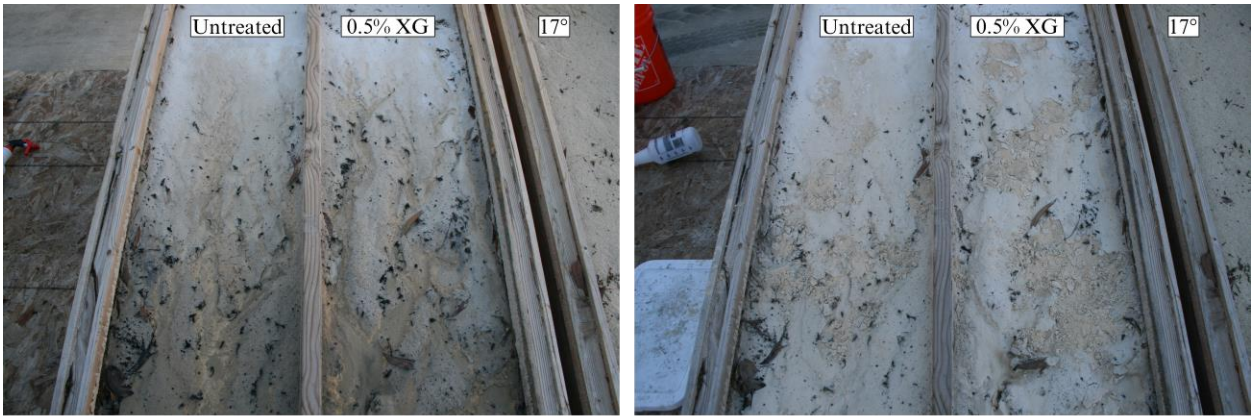

a. Fine sand morphology after RE 7 b. Raccoon prints prior to re-covering the slopes

Figure 2.4: Extreme channels formed in the fine sand slope with subsequent animal activity

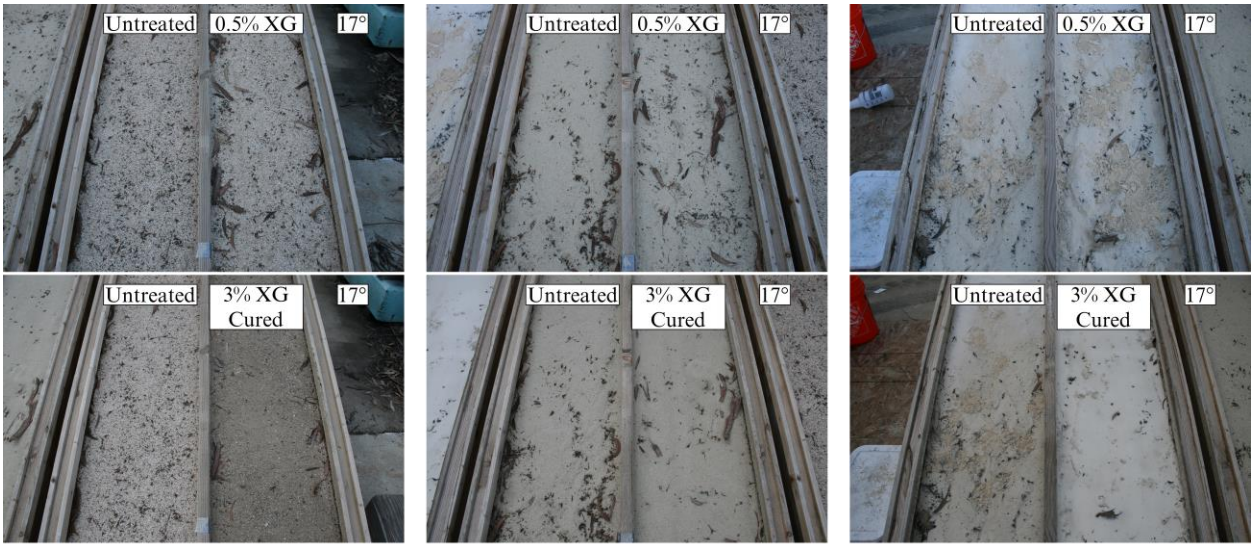

a. Coarse sand b. Medium sand c. Fine sand

Figure 2.5: 17° slopes before (top) and after (bottom) re-covering with cured 3% XG on November 22, 2021

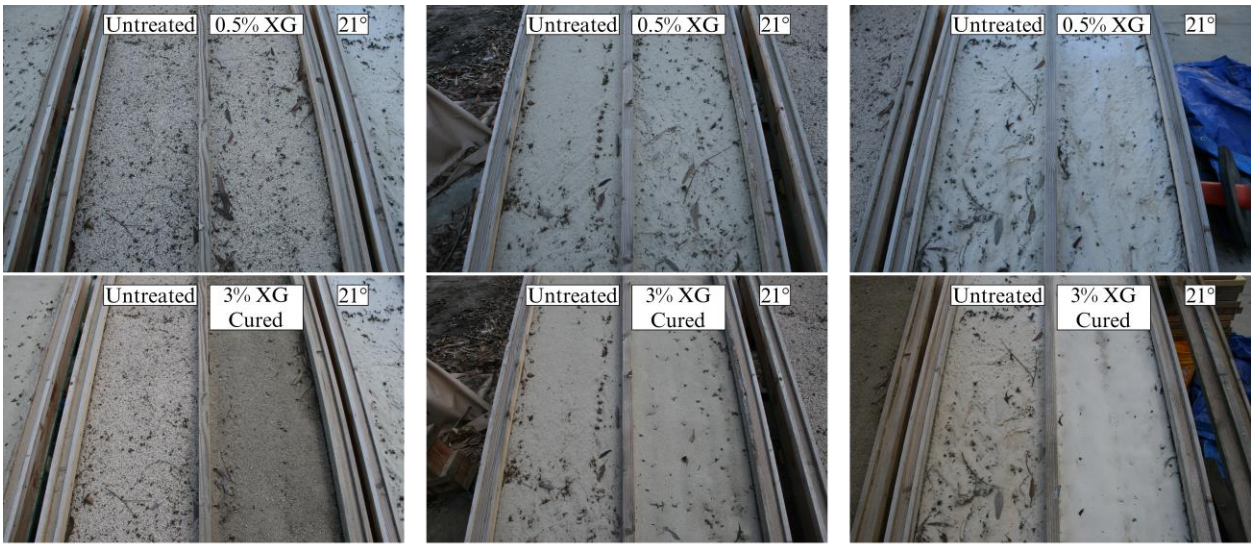

a. Coarse sand b. Medium sand c. Fine sand

Fig. 2.6: 21° slopes before (top) and after (bottom) re-covering with cured 3% XG on November 22, 2021

morphology after RE 8 in Figure 2.7 reveal that the erosion followed the same pattern, with most of the flow diverting into the pre-formed channels and chipping away the cured layer at those sections. Figure 2.7 also shows the state of the slopes during the last two REs. The surface morphology was not the only factor that led to enhanced erosion, as Figure 2.7b reveals that the XG treated flume had still not dried seven days later, three days before RE 9 with a rain intensity of 14.15 mm/hr and a rain duration of 166 min, due to the higher XG percentage and the colder

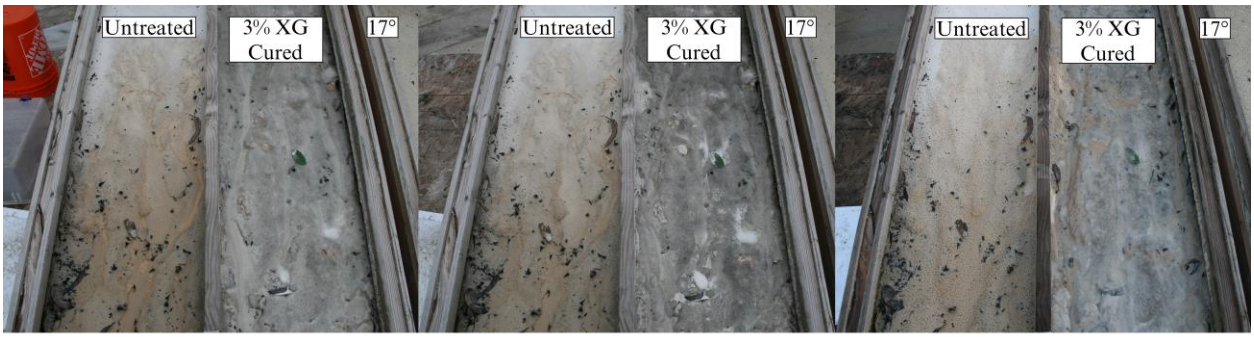

a. December 16, 2021, after RE 8 b. December 23, 2021, 3 days before RE 9 c. December 27, 2021, after RE 9

Figure 2.7: Enhanced erosion at pre-existent channels and over-saturated XG-sand mix

temperature observed in December. With the slopes over-wetted, the hardened crust layer remained in a gel state, allowing for entire sections along the pre-existing channels to erode swiftly. Figure 2.8 shows the final surface morphology of each slope.

2.3.2 Flows from Rain Events

2.3.2.1 Erosion and water runoff

As shown in Table 2, real-world rainstorms are uncontrolled events with the rain duration, average and 15-min peak rain intensities varying widely. Because of these variables changing from one storm to the next, erosion and water runoff may be assumed to not follow a trend, but when plotting the 15-min peak rain intensities along with both erosion (Figure 2.9a) and water runoff (Figure 2.9b), they both follow the trend of the rain intensities regardless of the duration that it rained. After the slopes are re-covered however, this ceases to be the case.

As for the treatment performance, Figure 2.9a shows that the 0.5% XG treated flumes for runoff for the treated flumes was also slightly more than observed for the untreated slopes. Once

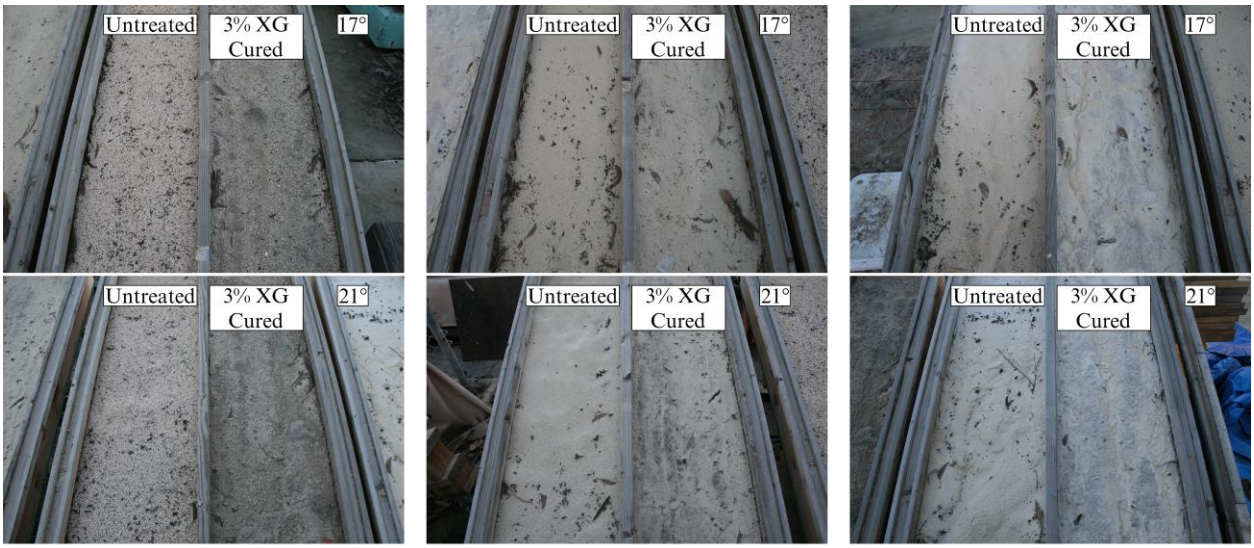

a. Coarse sand b. Medium sand c. Fine sand

Figure 2.8: Final surface morphology on February 4, 2022

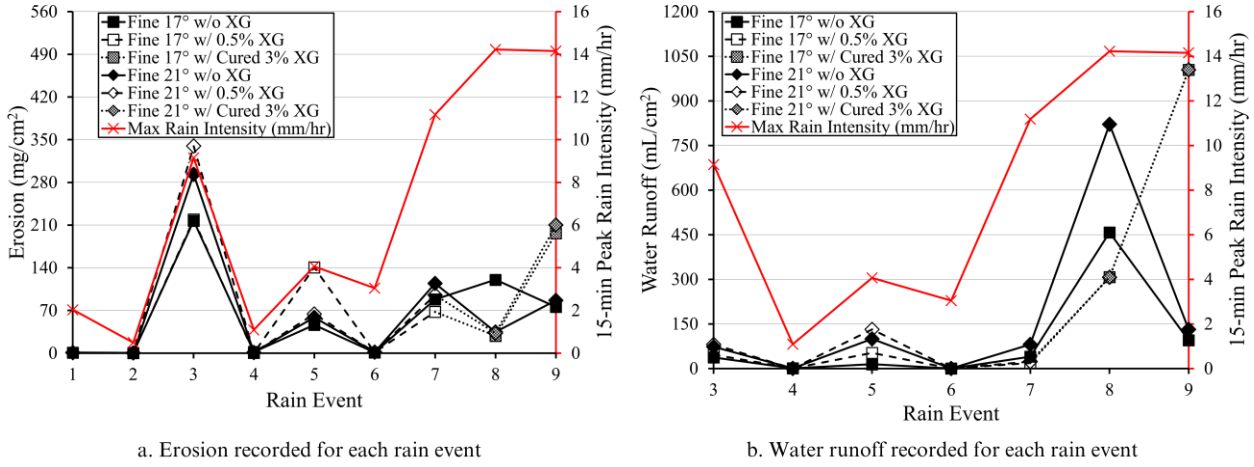

a. Erosion recorded for each rain event

b. Water runoff recorded for each rain event

Figure 2.9: Fine sand erosion and water runoff with the 15-min peak rain intensities

re-covered with the cured 3% XG-sand mix, the 17° treated slope performed much better, with 28.31 mg/cm^2 (283.1 g/m^2) eroded as opposed to 120.31 mg/cm^2 (1203.1 g/m^2) from the untreated flume during RE 8. The 21° treated slope performed only slightly better than its untreated counterpart when re-covered and cured with 3% XG. The final RE saw a large increase in erosion and water runoff for the XG-covered slopes due to the over-wetted conditions prior to the rain event.

For medium sand shown in Figure 2.10, the 0.5% XG slopes have reduced erosion during RE 3, but experience much more erosion in RE 5, with the 17° and 21° slopes experiencing 10.2 and13.6 times more, respectively, than the untreated slopes. The same trend is seen with the water runoff. After RE 3, there was little erosion in the untreated hydrophobic slopes. The water runoff stayed consistent with an increase, decrease, and another increase from RE to RE. After applying the cured 3% XG treatment, the slopes produced little change in erosion values but at a higher rain intensity than before, yet still more than the untreated slopes. The treated slopes then see a spiked increase in erosion during RE 9, much like the fine sand treated slopes. This is explained by the pre-formed channels from before the slopes were re-covered, with the enhanced erosion occurring

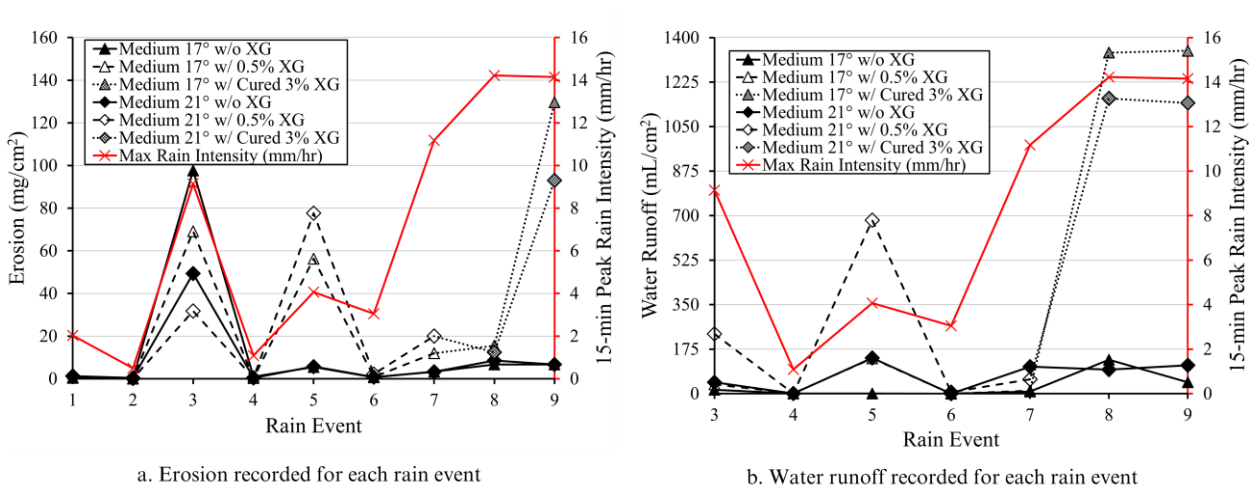

a. Erosion recorded for each rain event

b. Water runoff recorded for each rain event

Figure 2.10: Medium sand erosion and water runoff with the 15-min peak rain intensities

along those channels. Recall Figure 2.7b, showing the slopes were not completely dry from RE 8 when RE 9 occurred, leading the already saturated XG-sand mix to slide down in pieces instead of a hardened crust protecting the slope before being over-wetted.

Figure 2.11a shows that the 0.5% XG 17° containing coarse sand initially reduced erosion during RE 3, but produced more during RE 5, much like was seen with the medium sand treated slopes. Both treated angles yielded less erosion than the untreated slopes during RE 7 and

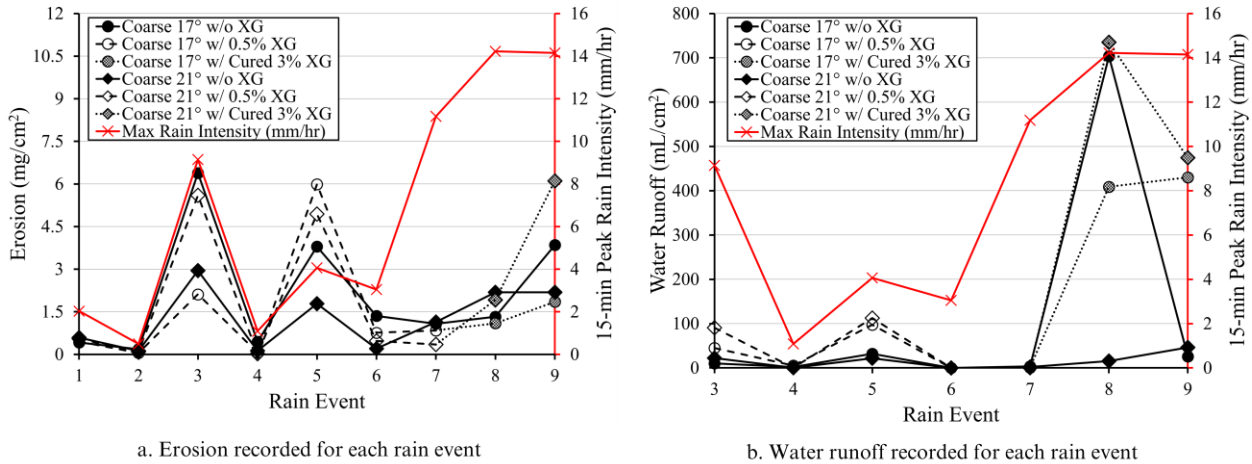

a. Erosion recorded for each rain event

b. Water runoff recorded for each rain event

Figure 2.11: Coarse sand erosion and water runoff data with the 15-min peak rain intensities

continued that trend after re-covering with cured 3% XG. Once again, there was an increase in erosion from RE 9, but not to a large extent as the largest increase was in the 21° treated slope, from 1.92 to 6.11 mg/cm^2 (19.2 to 61.1 g/m^2). During REs 3, 5 and 9, the water runoff produced from the treated slopes were higher.

2.3.2.2 Cumulative erosion and water runoff

Figures 2.12, 2.13, and 2.14 all compare the cumulative erosion and water runoff for each angle and treatment type for fine, medium, and coarse sand respectively. Focusing on the cumulative erosion for each sand type, the most erosion with the 0.5% XG treatment for fine sand occurred during RE 3, and during RE 5 for medium and coarse sand. As seen with the data collected each RE, the cumulative erosion shows the similarities in erosion trends when XG is used. For all sand types and both angles, the XG treated slopes follow the same trends but at different values, with the fine sand slopes eroding the most with a cumulative erosion of 700.35 mg/cm^2 (7003.5 g/m^2) averaged between the angles, coarse sand slopes the least with 16.63 mg/cm^2 (166.3 g/m^2), and medium sand slopes eroding in-between the two with 261.50 mg/cm^2

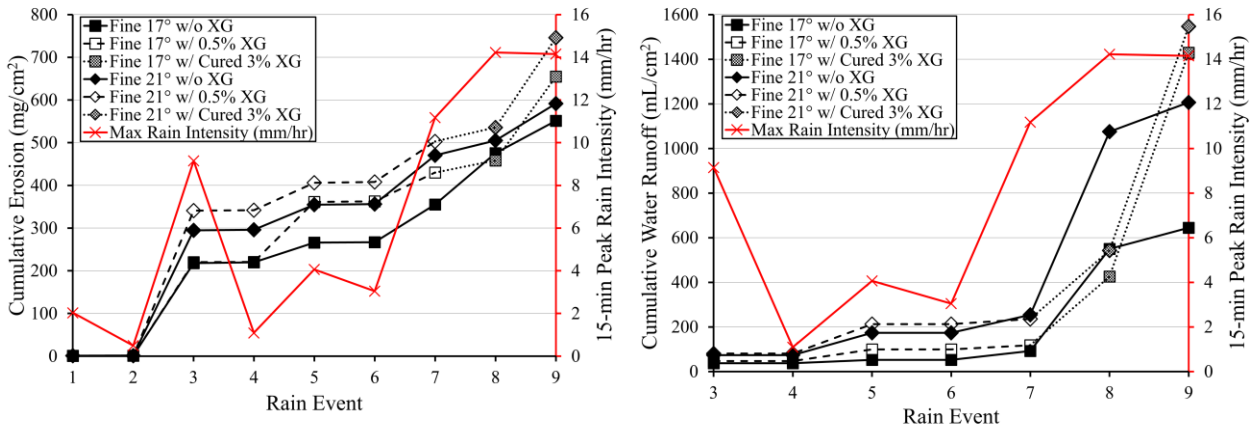

a. Cumulative erosion after each rain event

b. Cumulative water runoff after each rain event

Figure 2.12: Fine sand cumulative erosion and water runoff with the 15-min peak rain intensities

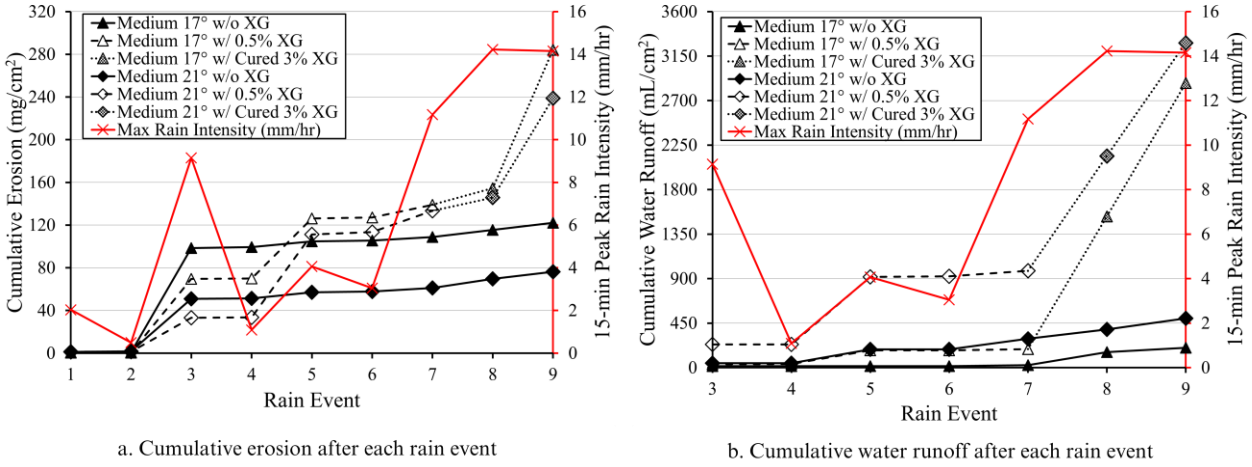

a. Cumulative erosion after each rain event

b. Cumulative water runoff after each rain event

Figure 2.13: Medium sand cumulative erosion and water runoff with the 15-min peak rain intensities

(2615.0 g/m^2). The untreated hydrophobic slopes do not have similar trends between each sand, however, except for the erosion from RE 3. While the cumulative figures show the untreated fine sand erosion increases from RE to RE with different slopes, the coarse cumulative trend is more linear. It can also be seen that after the initial erosion from RE 3, medium sand erosion is very little and very linear.

When comparing the cumulative water runoff for each sand, once again it can be seen that the water runoff follows a similar trend from sand to sand for untreated and 0.5% XG treated slopes, with the 0.5% XG 21° slope producing more overall water runoff during REs 3 and 5 but maintain the same trend. When the XG is increased to 3%, much higher water runoff was observed. It can be noted that the water runoff slopes between REs 8 and 9 go from steeper, linear, and shallower from fine, medium, and coarse sands. This is explained through the saturation of the slopes, where most of the fine sand slope was still over-saturated from the previous RE, and the coarse sand slopes were the least over-saturated slopes, allowing the XG-sand mixture to absorb water, producing less water runoff. For the XG treated slopes, those with medium sand accumulated the most water runoff, with 3079.58 mL/cm^2 (30795.8 L/m^2) averaged between the

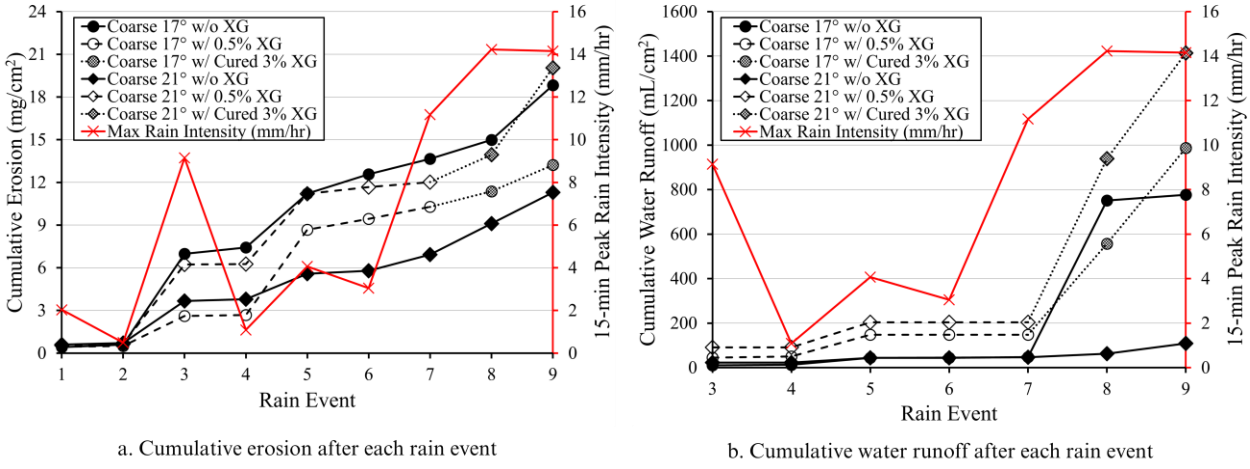

a. Cumulative erosion after each rain event

b. Cumulative water runoff after each rain event

Figure 2.14: Coarse sand cumulative erosion and water runoff with the 15-min peak rain intensities

angles, fine sand slopes, less than half of the medium slopes, producing 1488.10 mL/cm^2 (14881.0 L/m^2), and the least were coarse sand slopes with 1200.11 mL/cm^2 (12001.1 L/m^2).

2.4 CONCLUSIONS

With natural rain events, debris from trees, and animal activity interacting with the hydrophobic slopes, the study offers real-world performance after the application of XG-sand mixtures as a slope stability mitigation technique. The results validate results from Chapter 1 which found that an uncured 0.5% XG-sand mix produced more erosion than an untreated hydrophobic slope. Also, while cured 3% XG-sand mixes greatly reduce erosion on flat, non-eroded slopes, the same mix does not reduce erosion when applied to slopes with pre-existing channels.

The low rain intensities from REs 1 and 2 wetting and allowing the surfaces of the slopes to cure provided a hardened layer which eroded almost the same amount as the untreated slopes and provided more water runoff due to reduced infiltration from the XG bonds. With a higher percentage of XG used to provide stronger bonds between the particles, the initial rain events

would produce less erosion and more water runoff due to the higher concentration of XG present filling gaps between the particles.

While cured 3% XG-sand mixes were found to reduce surface erosion for non-eroded slopes, when applied to slopes with pre-existing channels, erosion was increased from the untreated slopes. This is an important note as application on burned slopes in nature where there are channels already from previous erosion can greatly affect the performance. In these cases, it is recommended to use percentages larger than 3% in the XG-sand mixture, but this must also be used cautiously considering the frequency of storms in the area and the temperature. This is because with 0.5% XG after RE 5, the slopes were completely dry three days later before RE 6 in early October. However, after 3% XG was applied and after RE 8 in mid-December, 12 days was not enough to completely dry the slopes, resulting in greatly increased erosion during RE 9.

Using XG as a slope stability technique also provides similar erosion trends for all three sand types tested, with fine sand slopes eroding the most, medium sand slopes next, and the least were the coarse sand slopes. Very similar trends were found between each sand type for the collected water runoff, with coarse sand slopes producing the least, fine sand slopes slightly more than coarse, and more than double the water runoff in fine sand slopes were observed with the medium sand slopes.

Acknowledgements

Chapter 2, in part, is currently being prepared for submission for publication of the material. Chavez De Rosas, Jonathon; Tomac, Ingrid. The thesis author was the primary researcher and author of this material.

REFERENCES

Akin, I. D., Garnica, S. S., Robichaud, P. R., and Brown, R. E. (2021). "Surficial stabilization of wildfire-burnt hillslopes using xanthan gum and polyacrylamide." *Geotech. Geol. Eng.* DOI: 10.1007/s10706-021-01951-4.

Akin, I. D. and Likos, W. J. (2016). "Water vapor sorption of polymer-modified bentonites." *Geo-Chicago 2016,* ASCE, Reston, VA, 508–517. DOI: 10.1061/9780784480144.050.

Alexandre, M. and Dubois, P. (2000). "Polymer-layered silicate nanocomposites: preparation, properties and uses of a new class of materials." *Materials Science and Engineering: R: Reports,* 28(1), 1–63.

Ayeldeen, M. K., Negm, A. M., and El Sawwaf, M. A. (2016). "Evaluating the physical characteristics of biopolymer/soil mixtures." *Arab. J. Geosci.,* 9(5), 371–384. DOI: 10.1007/s12517-016-2366-1.

Cabalar, A., Wiszniewski, M., and Skutnik, Z. (2017). "Effects of xanthan gum biopolymer on the permeability, odometer, unconfined compressive and triaxial shear behavior of a sand." *Soil Mech. Found. Eng.*, 54(5), 356–361. DOI: 10.1007/s11204-017-9481-1.

Carvalho, S. C. P., de Lima, J. L. M. P., and de Lima, M. I. P. (2014). "Using meshes to change the characteristics of simulated rainfall produced by spray nozzles." *International Soil and Water Conservation Research*, 2(2), 67–78. DOI: 10.1016/S2095-6339(15)30007-1.

Chen, R., Lee, I., and Zhang, L. (2015). "Biopolymer stabilization of mine tailings for dust control." *J. Geotech. and Geoenviron. Eng.*, 141(2), 04014100. DOI: 10.1061/(ASCE)GT.1943-5606.0001240.

CNRFC and NOAA (2021). *CNRFC Data Archive,* <https://www.cnrfc.noaa.gov/arc_search.php>.

Crockford, H., Topalidis, S., and Richardson, D. P. (1991). "Water repellency in a dry sclerophyll eucalypt forest — measurements and processes." *Hydrol. Process.,* 5(4), 405–420. DOI: 10.1002/hyp.3360050408

DeBano, L. F. (1967). *Soil Wettability and Wetting Agents: Out Current Knowledge of the Problem,* Vol. 43. Pacific Southwest Forest and Range Experiment Station, Forest Service, US Department of Agriculture.

DeBano, L. F. (1981). *Water repellent soils: a state-of-the-art,* Vol. 46. US Department of Agriculture, Forest Service, Pacific Southwest Forest and Range Experiment Station.

DeBano, L. F. and Krammes, J. S. (1966). "Water repellent soils and their relation to wildfire temperatures." *Hydrological Sciences Journal*, 11(2), 14–19.

Department of Forestry and Fire Protection (2022). "Stats & events." *Cal Fire*, <https://www.fire.ca.gov/stats-events/>.

Doerr, S. H., Shakesby, R. A., and Walsh, R. P. D. (1996). "Soil hydrophobicity variations with depth and particle size fraction in burned and unburned eucalyptus globulus and pinus pinaster forest terrain in the Agueda Basin, Portugal." *Catena*, 27(1), 25–47.

Doerr, S. H., Shakesby, R. A., and Walsh, R. P. D. (2000). "Soil water repellency: its causes, characteristics and hydro-geomorphological significance." *Earth-Science Reviews*, 51(1-4), 33–65.

Gioia, F. and Ciriello, P. P. (2006). "The containment of oil spills in porous media using xanthan/aluminum solutions, gelled by gaseous CO_2 or by $AlCl_3$ solutions." *Journal of Hazardous Materials*, 138(3), 500–506.

Ham, S.-M., Chang, I., Noh, D.-H., Kwon, T.-H., and Muhunthan, B. (2018). "Improvement of surface erosion resistance of sand by microbial biopolymer formation." *J. of Geotech. and Geoenviron. Eng.*, ASCE, 144(7), 06018004. DOI: 10.1061/(ASCE)GT.1943-5606.0001900.

Helvey, J. D. (1980). "Effects of a north central Washington wildfire on runoff and sediment production." *JAWRA Journal of American Water Resources Association*, 16(4), 627–634.

Huffman, E. L., MacDonald, L. H., Stednick, J. D. (2001). "Strength and persistence of fire-induced soil hydrophobicity under ponderosa and lodgepole pine, Colorado Front Range." *Hydrol. Process.*, 15(15), 2877–2892. DOI: 10.1002/hyp.379.

Joga, J. R. and B. J. S., V. (2020). "Effect of xanthan gum biopolymer on dispersive properties of soils." *World Journal of Engineering*, 17(4), 563–571.

Kavazanjian Jr., E., Iglesias, E., and Karatas, I. (2009). "Biopolymer soil stabilization for wind erosion control." *Proceedings of the 17th International Conference on Soil Mechanics and Geotechnical Engineering (Volumes 1, 2, 3 and 4)*, IOS press, 881–884. DOI: 10.3233/978-1-60750-031-5-881.

Khachatoorian, R., Petrisor, I. G., Kwan, C.-C., and Yen, T. F. (2003). "Biopolymer plugging effect: laboratory-pressurized pumping flow studies." *Journal of Petroleum Science and Engineering*, 38(1-2), 13–21.

Lee, S., Im, J., Cho, G.-C., and Chang, I. (2019). "Laboratory triaxial test behavior of xanthan gum biopolymer-treated sands. " *Geomechanics and Engineering*, 17(5), 445–452.

Mahamaya, M., Das, S. K., Reddy, K. R., and Jain, S. (2021). "Interaction of biopolymer with dispersive geomaterial and its characterization: An eco-friendly approach for erosion control." Journal of Cleaner Production, 312, 127778. DOI: 10.1016/j.jclepro.2021.127778.

Meeuwig, R. O. (1971). *Infiltration and water repellency in granitic soils*, Vol. 111. Intermountain Forest & Range Experiment Station, Forest Service, US Department of Agriculture.

Moghal, A. A. B., Vydehi, K. V. (2021). "State-of-the-art review on efficacy of xanthan gum and guar gum inclusion on the engineering behavior of soils." *Innovative Infrastructure Solutions*, 6(2), 1–14. DOI: 10.1007/s41062-021-00462-8.

Movasat, M. and Tomac, I. (2020). "Evaluation and remediation of post-wildfire slope stability." *E3S Web of Conferences*, Vol. 205, EDP Sciences, 04007. DOI: 10.1051/e3sconf/202020504007.

NOAA (2011). *National Weather Service Glossary: Closed Low*, <https://forecast.weather.gov/glossary.php?word=closed+low>.

Oakley, N. S., Lancaster, J. T., Kaplan, M. L., Ralph, F. M. (2017). "Synoptic conditions associated with cool season post-fire debris flows in the Transverse Ranges of southern California." *Natural Hazards*, 88(1), 327–354. DOI: 10.1007/s11069-017-2867-6.

Oakley, N. S., Redmond, K. T. (2014). "A Climatology of 500-hPa Closed Lows in the Northeastern Pacific Ocean, 1948–2011." *Journal of Applied Meteorology and Climatology*, 53(6), 1578–1592. DOI: 10.1175/JAMC-D-13-0223.1.

Ralph, F. M., Prather, K. A., Cayan, D., Spackman, J. R., DeMott, P., Dettinger, M., Fairall, C., Leung, R., Rosenfeld, D., Rutledge, S., Waliser, D., White, A. B., Cordeira, J., Martin, A., Helly, J., Intrieri, J. (2016). "CalWater Field Studies Designed to Quantify the Roles of Atmospheric Rivers and Aerosols in Modulating US West Coast Precipitation in a Changing Climate." *Bulletin of the American Meteorological Society*, 97(7), 1209–1228. DOI: 10.1175/BAMS-D-14-00043.1.

Savage, S. M. (1974). "Mechanism of fire-induced water repellency in soil." *Soil Science Society of America Journal*, 38(4), 652–657.

Scott, D.F. and Van Wyk, D. B. (1990). "The effects of wildfire on soil wettability and hydrological behavior of an afforested catchment." *Journal of Hydrology*, 121(1-4), 239–256.

Soldo, A., Miletić, M., Auad, M. L. (2020). "Biopolymers as a sustainable solution for the enhancement of soil mechanical properties." *Scientific Reports*, 10(1), 1–13. DOI: 10.1038/s41598-019-57135-x.

Tiwari, B., Ajmera, B., Gonzalez, A., Sonbol, H. (2020). "Impact of Wildfire on Triggering Mudslides—A Case Study of 2018 Montecito Debris Flows." *Geo-Congress*

2020: Engineering, Monitoring, and Management of Geotechnical Infrastructure, ASCE, Reston, VA, 40–49.

Tran, A. T. P., Chang, I., Cho, G.-C. (2019). "Soil water retention and vegetation survivability improvement using microbial biopolymers in drylands." *Geomechanics and Engineering*, 17(5), 475–483.